AN EXPERIMENTAL INVESTIGATION OF THE PURE BENDING CHARACTERISTICS OF SQUARE STRUCTURAL STEEL TUBING

A Dissertation

Presented to

the Faculty of the Department of Civil Engineering

The University of Houston

In Partial Fulfillment

of the Requirements for the Degree

Doctor of Philosophy in Civil Engineering

---

by

Ray Rolland Ayers

December 1973

ACKNOWLEDGEMENTS

I should like to offer my thanks to Dr. James M. Nash for the special way he has guided my research efforts. I shall treasure our association leading to this dissertation.

For the confidence he has shown during my degree work, I am indebted to Dr. Ardis White. I wish to express my gratitude to the other members of my dissertation committee, Dr. O. I. Ghazzaly, Dr. W. J. Graff, Professor L. J. Castellanos and Dr. P. G. Hedgcoxe.

To Shell Pipe Line Corporation and Shell Development Company I acknowledge the financial assistance given to me through the Educational Assistance Program for employees. I appreciate the many ways my friends at the Pipeline Research and Development Laboratory have helped me. Special thanks is due to Mr. James Smith and Mr. Dean Henning who helped me assemble the experimental apparatus and instrumentation.

I dedicate this work to my wife Carolyn, and our children Cheryl Ann, Tommy and Andy whom I love very much.

AN EXPERIMENTAL INVESTIGATION OF THE PURE BENDING CHARACTERISTICS OF SQUARE STRUCTURAL STEEL TUBING

An Abstract

Presented to

the Faculty of the Department of Civil Engineering

The University of Houston

In Partial Fulfillment

of the Requirements for the Degree

Doctor of Philosophy in Civil Engineering

---

by

Ray Rolland Ayers

December 1973

ABSTRACT

Hot-rolled structural steel rectangular tubing has, in recent years, become an attractive and a structurally efficient construction material. Structural tubing, like other thin-walled materials, fails in bending with a collapse of the cross-section before the ultimate bending capacity is achieved. This investigation explores the pure bending characteristics of square structural steel tubing. Importance is placed on determining the maximum resisting moment of the cross-section as well as the corresponding curvature. The experimental investigation, in which experimental stress analysis techniques were chosen to obtain specific measurement objectives, involved eighteen tests of six specimen groups. Two theoretical approaches, found in the literature and adapted to the square tube, were compared with the experimental results.

The experimental study revealed that a flange buckling failure mode, characteristic of a thin-tube assumption, was applicable for a tube width-to-thickness ratio as low as 25. The inelastic buckling theory adapted from that proposed by Rhodes and Harvey was found to apply for thin tubes. For thicker tubes, a valid comparison of the distortion theory developed by Ades was impossible. Unexpected residual strains in excess of 0.1% were found in the walls of the mill-formed tubing.

TABLE OF CONTENTS

CHAPTER PAGE

LIST OF TABLES

LIST OF FIGURES

LIST OF SYMBOLS

A cross-sectional area

B width of square tube, outside dimensions

b width of square tube, centerline dimensions

b_e effective width

$\bar{C}$ dimensionless curvature

D plate modulus of rigidity

E Young's modulus

E_s secant modulus

e_i equivalent uniaxial strain

I second moment of the cross-section

I' reduced second moment

i index number

j index number

K buckling constant

M resisting moment

$\bar{M}$ dimensionless moment

M_{MAX} maximum moment

M_{yld} yield moment based on 0.5 percent strain

n Ramberg-Osgood slope parameter

Q maximum first moment of the cross-section

R initial radius of a curved beam

R_t transverse radius of distorted web

s tube perimeter coordinate

t tube wall thickness

U strain energy density

W total work

w flange lateral deflection

w_o constant

w_1 constant

w_i distortion of tube wall at node i

x coordinate axis

x_i x-coordinate of node i

y coordinate axis

$\bar{y}$ distance from neutral axis to extreme fiber

y_i y-coordinate of node i

$\bar{\beta}$ reduction factor

β_i angle of distorted tube wall at node i

γ wall thickness coordinate

$\bar{\Delta}$ dimensionless distortion

δ fractional wall thickness parameter, deflection

ϵ strain

ϵ_{cR} critical buckling strain

ϵ_L longitudinal strain

ϵ_{PL} strain at proportional limit

ϵ_{T} transverse strain

λ dimensionless parameter

μ Poisson's ratio

$\bar{\mu}$ inelastic form of Poisson's ratio

ρ deformed radius of curvature

ρ_{CR} critical value of the deformed radius of curvature

σ stress

σ_{CR} critical buckling stress

σ_{i} stress corresponding to e_i

σ_{MAX} maximum stress

σ_{ULT} ultimate stress

σ_{yld} yield stress at a strain of 0.5 percent

$\sigma_{0.7}$ Ramberg-Osgood stress parameter

CHAPTER I

INTRODUCTION

Elementary beam theory is based on assumptions of linearly-elastic material characteristics and negligible cross-sectional distortion. When thin-walled, closed-section beams are subject to bending loads there can be a discernable distortion of the cross-section. As a result of this distortion, the beam is much more flexible than one would predict by neglecting such an effect. Von Karman (1)*analyzed the case of the elastic bending of a circular tube, including the distortion effects, in the early 1900's. Timoshenko (2) made a similar study of a curved, rectangular tube in 1923.

In recent years there has been a distinct trend toward designing beams based on their ultimate, or maximum bending capacity as contrasted with earlier designs based on elastic theory. Such ultimate strength concepts were based on minimum weight criteria for such structures as aircraft and spacecraft, where excessive weight reduces the efficiency of the design. The search for more efficient beams has created the need for analytical techniques for describing the bending of thin-walled beams, including the effects of distortion of the cross-section, where loads are in excess of the elastic capacity of the material.

---

*Numbers in parentheses refer to same numbered references in the Bibliography.

Ades (3) proposed a technique for analyzing round tubes assuming that the cross-section distorts in the form of an ellipse. In that his technique is simple and in that results agree with experimental data, the Ades method satisfies the need for analysis of the circular tube.

The problem of the inelastic bending of a rectangular tubular member, accounting for distortion effects, has not been treated in the literature. There is a need for such an investigation because of the ever-increasing use of square and rectangular tubing in the construction of a multiplicity of structures. The increased use of rectangular tubing has been attributed to (a) the simplicity of effecting a tube-to-tube joint and (b) the desirability of having flat surfaces for attaching covering materials, as compared with a circular tube section.

This investigation is addressed to the problem of analyzing the inelastic bending characteristics of square structural steel tubing. Of particular interest is the transition range where tubes can no longer be considered as being thin-walled, and where the failure mode changes from one of inelastic buckling to one of a material failure with an accompanying distortion of the cross-section.

In the case of the circular tube Ades (3) found that a smooth transition from a buckling failure to a material failure with ovalization of the cross-section occurs in the vicinity of a tube width-to-wall-thickness ratio, D/t, of 50. For a D/t above 50 the failure mode is primarily a buckling one, while below 50 the mode is essentially a material one with ovalization.

The objectives of this investigation are as follows:

1. To experimentally identify the buckling-distortion transition range

for the specific case of mill-formed structural steel tubing having a square cross-section and a uniform wall thickness.

2. To provide experimental data for verifying candidate theories for use in the transition range.

3. To adapt theoretical techniques available in the literature to the solution of the square tube problem.

CHAPTER II

PREVIOUS WORK

The earliest published work on square or rectangular tubing is that of Timoshenko (2) in 1923. He studied the elastic bending stresses in curved tubes of rectangular cross-section. Timoshenko assumed a frame-type distortion shape for the cross-section and obtained an approximate solution by calculating the potential energy of deformation.

Referring to Figure 1, Timoshenko assumed that the deflection of flange elements "mn" and "qt" could be written in the form

$$w = w_0 \sin \frac{\pi x}{b} + w_1 \left(1 - \cos \frac{2\pi x}{b}\right) \tag{2.1}$$

where

x = axis at the flange centerline

b = flange width, centerline dimensions

w = flange lateral deflection

w_0, w_1 = constants to be determined.

A relation between these constants is found by considering a unit section as a rigid frame such that the webs are arcs of a circle.

The potential energy of deformation of the cross-section "mnqt" then consists of the potential energy of extension and compression normal to the

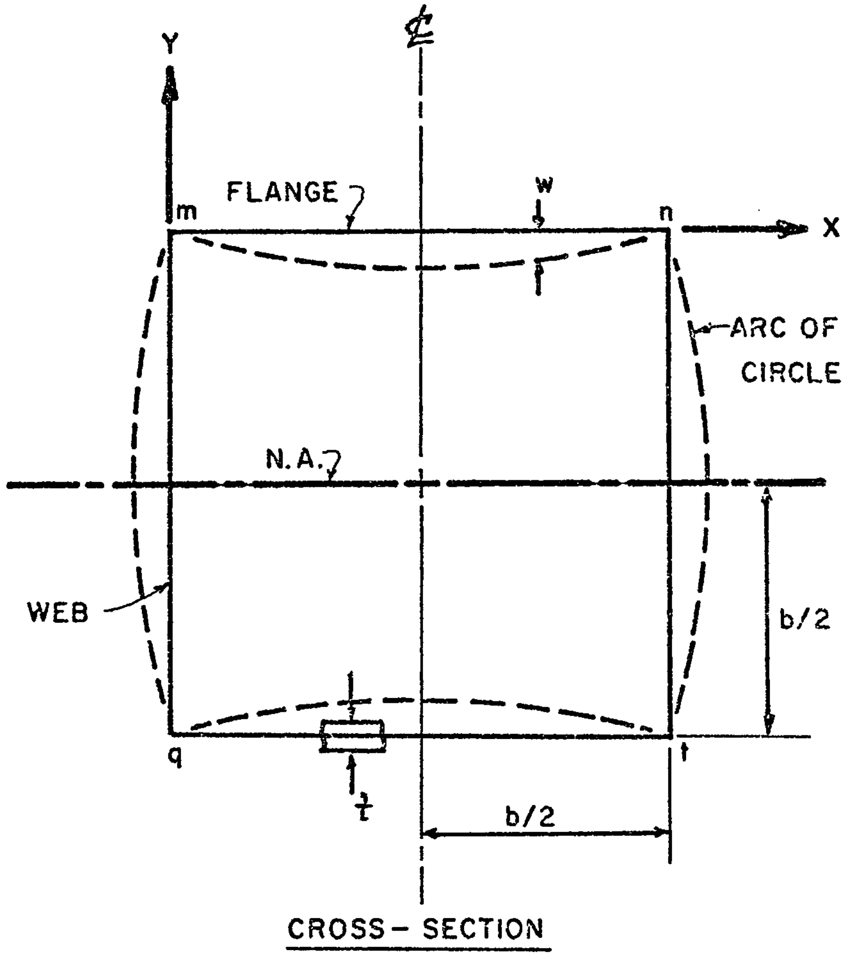

Figure 1. Geometry of the Timoshenko Square Tube Beam.

cross-section, plus the potential energy of bending in the frame. The form of the distortion of the cross-section must be that which will minimize the potential energy of deformation.

Timoshenko determined a "reduced" moment of inertia which takes into account the distortion of the cross-section,

$$I' = \bar{\beta} I \tag{2.2}$$

where

I' = reduced moment of inertia

I = second moment of the cross-sectional area

$\bar{\beta} \leq 1$ is the reduction factor given by

$$\bar{\beta} = 1 - f(R, t, b, \mu) \tag{2.3}$$

where

R = beam radius

t = tubular beam wall thickness

b = tube wall width, centerline dimensions

μ = Poisson's ratio.

This procedure leads to the following expression for in the case of a curved, square-tube beam of constant cross-section,

$$\bar{\beta} = \frac{49.18 + 1.332\lambda}{49.18 + 3.232\lambda} \tag{2.4}$$

where

$$\lambda = b^4/R^2t^2. \tag{2.5}$$

For a tube with a given b/t, the smaller the radius of curvature, the greater the effect of distortion will be. On the other hand, as the beam approaches a straight configuration, $R \to \infty$, and the effect of distortion becomes negligible.

The present investigation differs from that of Timoshenko in that beams considered here are straight. Timoshenko's analysis, as well, is an elastic analysis while the present one accounts for inelastic material behavior.

A design method for the thin-gage square tube in bending is given by the American Iron and Steel Institute (4). The technique generally accounts for the fact that flat plate compression elements making up a beam cross-section can develop a local instability which is not catastrophic in nature for the overall section. Additional bending load increments are resisted by a redistribution of stresses over the cross-section. This occurs since an unstable element cannot resist additional increments of load with the same stress distribution as that prior to the onset of instability. The reduced efficiency of a buckled plate element is accounted for analytically by substituting an "effective" width in place of the actual width.

The strength of a single simply-supported plate element was first investigated by von Karman, et al (5) in 1932. He found that the effective width of a flat plate element can be expressed by

$$b_e = \left(\pi / \sqrt{12(1-\mu^2)}\right) \sqrt{\frac{E}{\sigma}}\, t \qquad (2.6)$$

where

b_e = effective flange width ($b_e \leq b$)

E = Young's modulus

σ = compressive stress

μ = Poisson's ratio

b = plate width.

For a Poisson's ratio of 0.3 the former expression becomes

$$b_e = 1.9\sqrt{\frac{E}{\sigma}} \qquad (2.7)$$

The effective width at the ultimate loading condition is found by replacing σ by σ_{yld}, which is the compressive yield strength.

In 1940 Winter (6) published an experimental analysis of the effective widths of flanges of wide, thin-walled steel beams. Winter tested beams made up of flat plate elements and found that for most steel beams of this type the effective width of the compressive flange could be approximated

$$b_e = 1.9\sqrt{\frac{E}{\sigma_{MAX}}}\left[1 - 0.475\frac{t}{b}\sqrt{\frac{E}{\sigma_{MAX}}}\right] \qquad (2.8)$$

where

σ_{MAX} = compressive element edge stress

and the other symbols have been defined previously.

Cozzone (7) in 1943 published a method for determining the bending strength of a beam in the inelastic range. This method can be utilized to determine the maximum resisting moment of a given cross-section, such as a square tube, provided that distortion as well as local buckling is negligible. Assuming a stress distribution as shown in Figure 2, the maximum resisting moment is

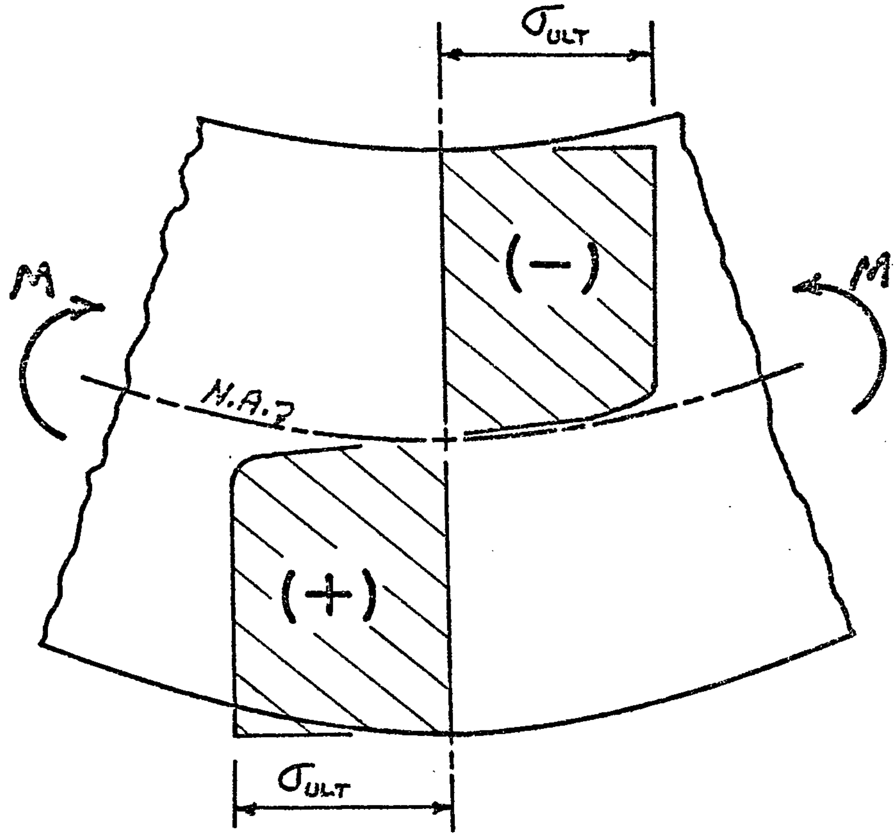

Figure 2. Stress Assumption for Determining the Maximum Resisting Moment.

$$M = 2\sigma_{ULT}\,Q \qquad (2.9)$$

where

M = maximum resisting moment

σ_{ULT} = ultimate stress of the material

Q = maximum first moment of the cross-section.

The assumptions involved in this analysis are that the tensile and compressive stress-strain properties are identical, and that the cross-section is generally rectangular.

The expression for the maximum resisting moment for a thick-walled square-tube beam becomes expanding Equation 2. 9,

$$M = \sigma_{ULT}\,Bt\left[3B/2 \;\; -3t\right] \qquad (2.10)$$

where

B = outside width of the square tube

and where the other symbols have been previously defined.

Returning to the light-gage beam design method, Rhodes and Harvey (8) proposed an alternative approach to that by Winter. They claimed that a failing of Winter's method is that there is no direct relationship between the applied moment and the effective width of the flange; consequently an iteration must be utilized. In the Rhodes-Harvey technique iteration is avoided.

The approach involves describing the critical stress to cause buckling of the compressive flange

$$\sigma_{CR} = \frac{K\pi^2 D}{b^2 t} \qquad (2.11)$$

where

σ_{CR} = buckling stress

K = buckling constant

b = flange width (centerline dimension)

t = flange thickness

D = plate modulus of rigidity.

According to a more rigorous theoretical approach by Rhodes (9),

$$K = 5.39$$

approximately for the specific case of a square-tube beam.

Utilizing an empirical curve for the flange effective width from Harvey

$$b_e = \left(0.7 \frac{\sigma_{CR}}{\sigma} + 0.3\right) b \qquad (2.12)$$

where

b_e = effective flange width

σ_{CR} = critical buckling stress

σ = applied stress.

one can then compute directly the effective square-tube section properties for a given stress intensity.

Concerning the post-buckling collapse failure of a square-tube beam, it is possible that a significant amount of inelastic activity can occur prior to the complete collapse of the cross-section. This effect can be accounted for, according to Rhodes and Harvey (8), by substituting the following effective width relation for that in Equation 2.12:

$$b_e = \left(0.7 \epsilon_{CR}/\epsilon + 0.3\right) b \qquad (2.13)$$

in which stresses are replaced by strains. Note that Equations 2.13 and 2.12 are identical for the elastic case. This latter expression takes into account the load-shedding in cases where $\sigma > \sigma_{yld}$, since b_e decreases while σ still equals σ_{yld}.

The method of Rhodes and Harvey is believed to show promise for investigating square-tube beams on the thin-walled side of the transition range.

No work is reported in the literature which addresses the problem of the inelastic bending of a square tube of a deformable cross-section. Steele (10) and Dwyer and Galambos (11) describe inelastic analyses of square tubes as torsional-flexural members and as beam-column members respectively, while Smith (12) addresses the post-buckling behavior of a box beam using an intricate tensor scheme. In all of these cases distortion of the cross-section is neglected.

Since circular tubes have historically received more analytical attention than rectangular ones, the literature on the inelastic bending of circular tubes of deformable cross-section was explored. It was expected that a technique for analyzing circular tubes of deformable cross-section might be modified for the square tube. Ades (3) in 1957 presented a method for calculating the total work done on a bent and deformed circular tube in the inelastic range. The principle of least work was used to determine the ovalization associated with the longitudinal curvature of the beam. The major assumption made in the analysis was that the deformation of the cross-section could be approximated as an ellipse which is constant along the beam length. A second assumption is that the tensile and compressive properties are identical. Thus, a simple tensile stress-strain curve can be utilized for determining the secant modulus in the inelastic range. The method also included an empirical expression for an inelastic form of Poisson's ratio.

CHAPTER III

THEORETICAL ANALYSES

Flange Buckling Analysis

Very light-gage square-tube sections show virtually no deformation of the cross-section as a whole, but buckling waves are observed to occur on the compressive flange along the beam. The Rhodes-Harvey (8) design procedure utilizes the concept of effective flange width as does the Winter (6) analysis used in the AISI design method (4). The benefit of the Rhodes-Harvey method is that a direct relation between the applied moment and the effective width is afforded. A comparison of this method with the Winter method and with experimental results supports its applicability.

A major change in the method developed here over the Rhodes-Harvey scheme is that the Ramberg-Osgood (13) stress-strain relations are incorporated. The calculation procedure is also changed in that the tube cross-section is broken into elements as defined in terms of nodal points, and a numerical procedure is employed allowing different material properties for each element depending on the state of stress of each.

In the local flange buckling analysis the grid system is established, shown in Figure 3. The nodal points for the numerical analysis as well as the corner approximations are indicated there. The typical tensile flange element between

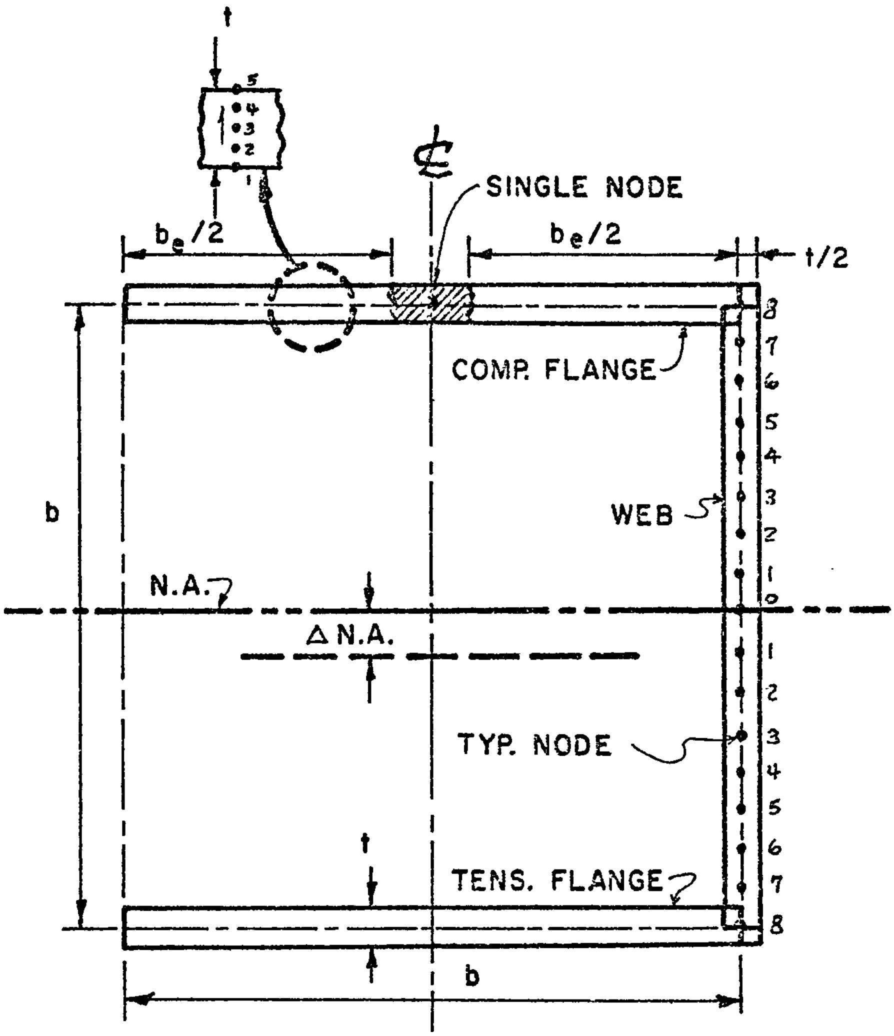

Figure 3. Grid System for the Flange Buckling Analysis.

two adjacent nodes has a thickness t and a length b. A typical web element has a thickness (width) t and a width (height) of b/16. The entire compressive flange is treated as a single element in keeping with the "effective-flange-width" buckling approach.

The first calculation determines the critical (elastic) local buckling strain by using (from Rhodes-Harvey (8))

$$\epsilon_{CR_{(E)}} = 4.8 \left(\frac{t}{b}\right)^2 \qquad (3.1)$$

where

$\epsilon_{CR_{(E)}}$ = critical elastic buckling strain

t = flange thickness

b = flange width, centerline dimensions.

Then the critical elastic strain is compared with the strain at which yielding occurs. The definition of yield stress utilized in this investigation is the stress magnitude at a yield strain of 0.5%. The smaller value of strain is used as the local buckling strain, ϵ_{CR} , in the analysis.

With a given value of curvature the longitudinal strain can be computed by

$$\epsilon_L = \bar{Y}/\rho \qquad (3.2)$$

where

ϵ_L = longitudinal strain

$\bar{Y}$ = distance from the neutral axis to the flange

ρ = radius of curvature.

If the longitudinal strain is less than critical, then the entire flange is effective. If, however, the longitudinal strain is larger, then an effective width calculation is called for. Again, following Rhodes and Harvey (8), the effective width equation is

$$b_e = \left(0.7\, \epsilon_{CR}/\epsilon_L + 0.3\right) b \tag{3.3}$$

where

ϵ_{CR} = critical buckling strain (elastic or inelastic)

b_e = effective flange width ($b_e \leq b$)

and other quantities are defined previously.

Once the effective width is used rather than the actual one, one must find the new neutral axis which is different from the axis of symmetry. The effective area is

$$\Sigma A_e = 3bt + b_e t \tag{3.4}$$

and the new centroidal distance becomes

$$\bar{Y}_e = \frac{\Sigma Ay}{\Sigma A_e} = 2bt/\Sigma A_e \tag{3.5}$$

where

ΣA_e = effective area of the entire section

ΣAy = first moment of the effective area

$\bar{Y}_e$ = flange ℄ distance from the effective neutral axis.

The longitudinal strain for any nodal point is simply the signed distance of the node from the neutral axis divided by the radius of curvature. The transverse strain is the negative product of the variable Poisson's ratio and the longitudinal strain. The stresses are computed using the method of Ades (3) based on the Ramberg-Osgood relations discussed more fully in the following section.

For each increment of curvature the stress distribution is computed and the resisting moment is determined as the integral of the stresses over the cross-sectional area. According to this theory the beam is said to collapse when the corners of the compressive flange yield.

A computer program (Appendix A) was used to perform the buckling theory computations. The program contains a subroutine used to perform the stress calculations.

Distortion Analysis

General

The general approach in deriving the distortion theory for the square tube is the same as that proposed by Ades (3). One must, however, develop new kinematic equations and make a different distorted shape assumption, since the problem is a square tube rather than a round one. The distortion assumption used in this investigation is that which Timoshenko used in his investigation of elastic, curved beams. Figure 1 shows Timoshenko's distortion assumption and Equation 2.1 is the governing transverse deflection relation. The accompanying assumption, it is recalled, is that the adjacent webs have rigid joints and that they deflect into the shape of an arc of a circle.

It is further assumed that the deformation of the cross-section is essentially that of frame bending where there is no change in the perimeter of the deformed shape when compared with the initial one. Other assumptions include negligible end effects and isotropic material behavior.

Internal Work

Ades (3) showed that the work of deformation can be calculated in both the elastic and inelastic ranges from the area under a standard stress-strain curve corresponding to an equivalent uniaxial strain

$$e_i = \sqrt{[1/(1-\bar{\mu}^2)][\epsilon_L^2 + \epsilon_T^2 + 2\bar{\mu}\epsilon_L\epsilon_T]} \qquad (3.6)$$

where

e_i = equivalent uniaxial strain

ϵ_L = biaxial longitudinal strain

ϵ_T = biaxial transverse strain

$\bar{\mu}$ = inelastic form of Poisson's ratio.

The incremental work per unit area for the constant distortion beam assumption is written as

$$dW = \frac{1}{2}\sigma_i e_i \, d\gamma \, ds \qquad (3.7)$$

where

dW = incremental work per unit area

σ_i = stress corresponding to the equivalent strain, e_i

$d\gamma$ = increment of wall thickness

ds = increment of tube wall width.

It is recognized that $\frac{1}{2}\sigma_i e_i$ is the area under the elastic portion of the stress-strain curve for a given equivalent uniaxial strain. Ades (3) further shows that the incremental work per unit area can be obtained in the elastic and inelastic ranges by computing the area under the stress-strain curve. The total work can then be obtained by computing the work per unit area at various points around the cross-section and through the tube wall and summing.

Principle of Least Work

The technique used is to assume that for a given curvature of the beam there is a unique distortion intensity which will render the internal work a minimum. This means that one can assume various magnitudes of distortion (using Equation 2.1) such that when plotted as the abcissa against the internal work of the cross-section, the curve so formed will contain a unique minimum point. This minimum point is the desired deformed shape magnitude. The process is then performed for each increment of curvature over the desired range of curvatures.

Numerical Integration

Knowledge of the deformed shape and its symmetry indicates that the numerical integration scheme need only be carried out for one-half of the cross-section: one quarter above the neutral axis and one quarter below. The section, although doubly symmetric in its undeformed shape, is not when deformed because of small changes in the state of stress and strain due to distortion. A grid network of nodes around the tube as well as through the tube walls is defined for the numerical computation process.

Geometry of Deformation

It is convenient to treat the web separately from the flange. Figure 4 shows the deformed geometry of the upper (compressive) half-web and Figure 5 shows that for the upper half-flange. The following kinematic relations describe the

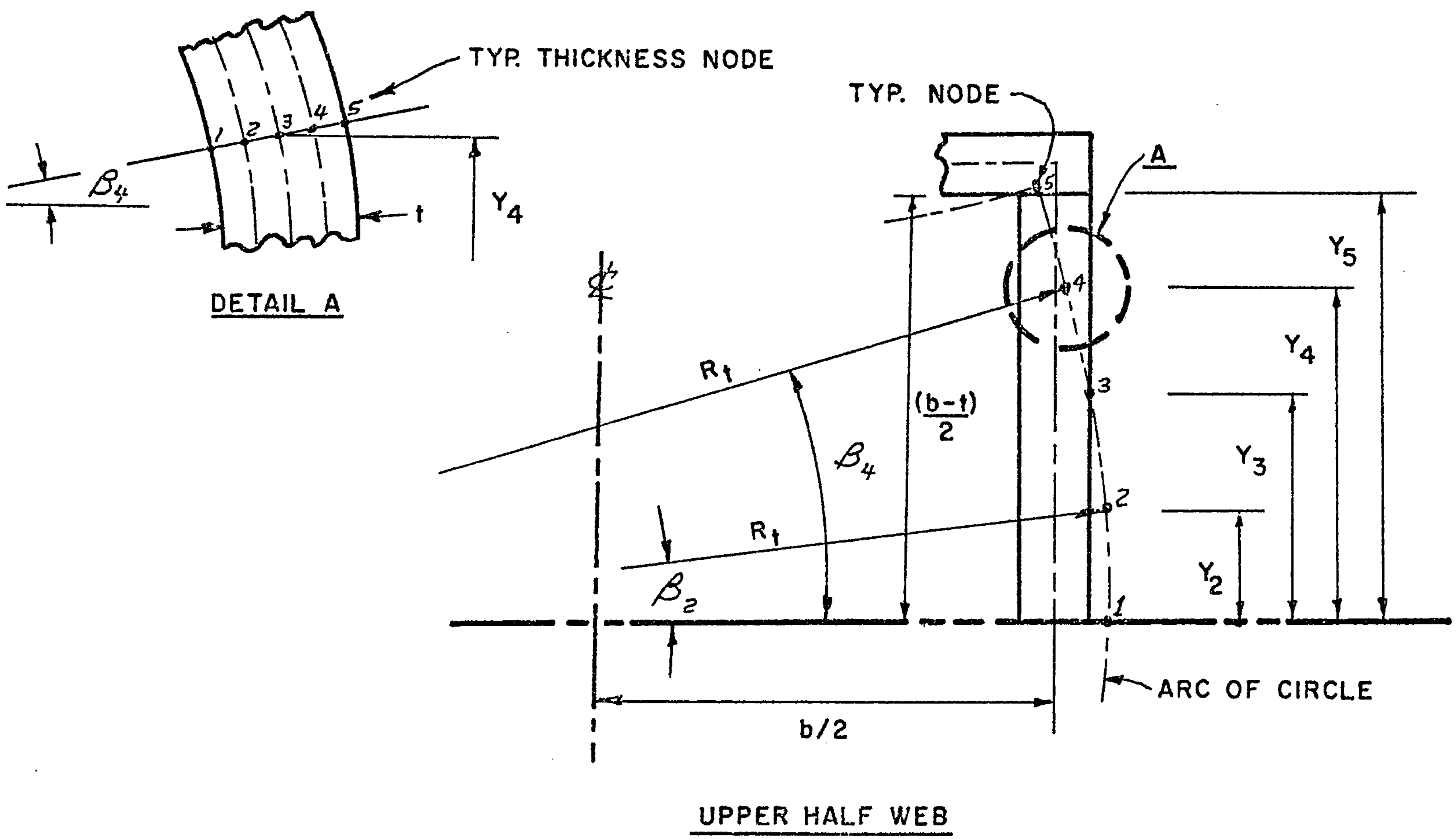

Figure 4. Grid System and Deformed Shape for the Web, Distortion Analysis.

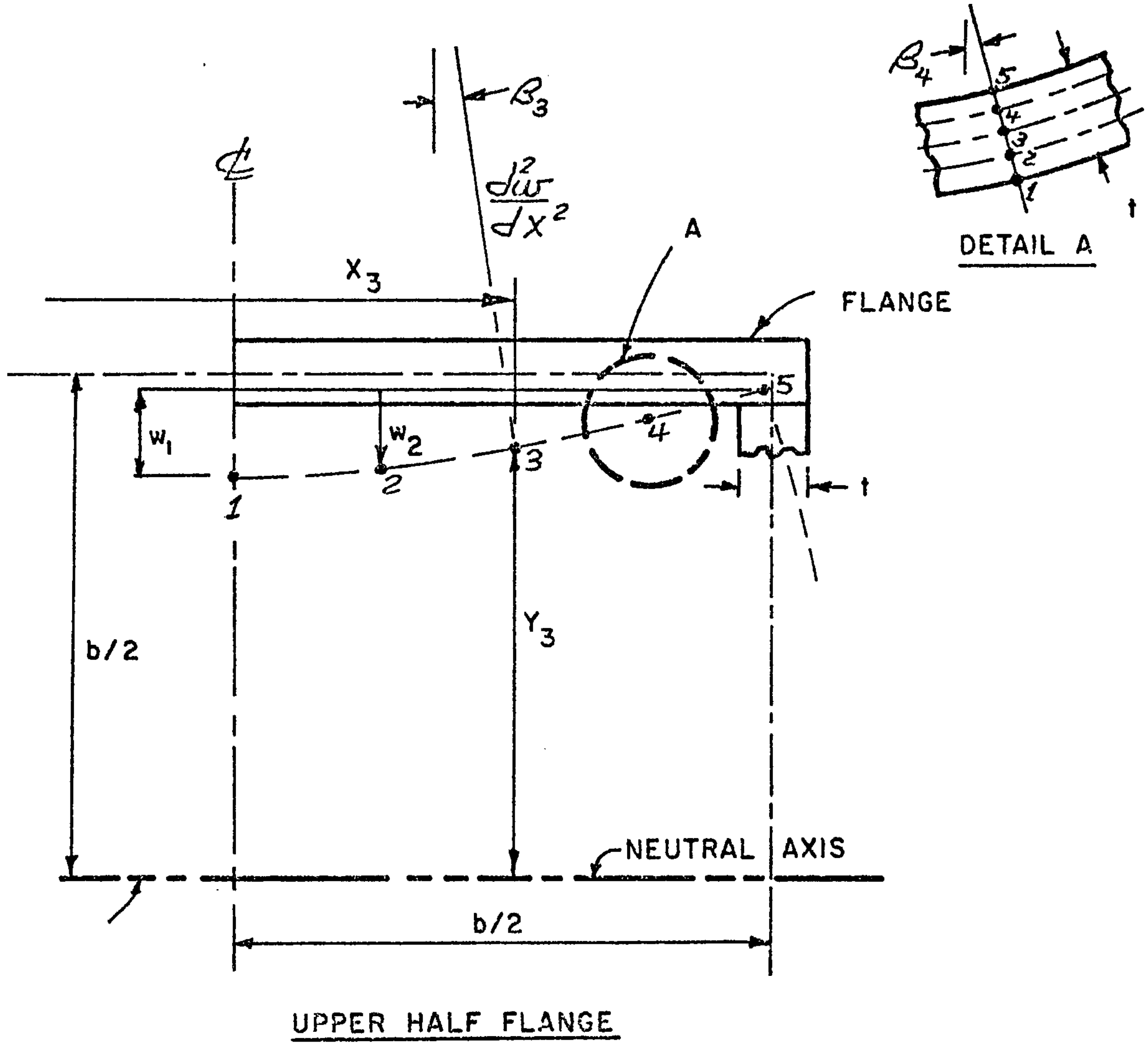

Figure 5. Grid System and Deformed Shape for the Flange, Distortion Analysis.

geometric conditions of the two figures.

For the web,

$$\beta_i = (i-1)(b-t)/8R_t \tag{3.8}$$

$$y_i = R_t \operatorname{Sin}(\beta_i) \tag{3.9}$$

$$R_t = b/t \Big/ \left(\frac{dw}{dx}\right)_{i=5} \tag{3.10}$$

and for the flange

$$w_i = w_o/1.3183\left[\operatorname{Sin}\left(\frac{\pi x_i}{b+t}\right) + \frac{1}{2\pi}\left(1-\operatorname{Cos}\left(\frac{2\pi x_i}{b+t}\right)\right)\right] \tag{3.11}$$

$$x_i = (b+t)/2 \;+\; (i-1)(b-t)/8 \tag{3.12}$$

$$\beta_i = \left(\frac{dw}{dx}\right)_i \tag{3.13}$$

$$y_i = R_t \operatorname{Sin}\left(\frac{b}{2R_t}\right) - w_i \tag{3.14}$$

where the web-flange intersection slope is

$$\left(\frac{dw}{dx}\right)_5 = -w_o/1.3183\left\{\operatorname{Cos}\frac{\pi(b+t/2)}{b+t} + \operatorname{Sin}\frac{2\pi(b+t/2)}{b+t}\right\}\frac{\pi}{b+t} \tag{3.15}$$

and the flange slope is

$$\left(\frac{dw}{dx}\right)_i = w_o/1.3183\left[\frac{\pi}{b}\operatorname{Cos}\left(\frac{\pi x_i}{b}\right) + \frac{1}{b}\operatorname{Sin}\left(\frac{2\pi x_i}{b}\right)\right] \tag{3.16}$$

and the other symbols are defined in the corresponding figures.

Once the deformed geometry is defined, the longitudinal and transverse strains may be determined. In the case of the web one must write an equation to define the increment of thickness, using the inner nodal point as the origin in each case

$$\delta_i = (i-1)\,t/4 - t/2 \tag{3.17}$$

where

δ_i = fractional wall thickness parameter

t = tube wall thickness

i = nodal thickness index, i = 1, 2, . . . 5.

The web longitudinal strain becomes (from Equations 3.8 - 3.10 and 3.17):

$$\epsilon_{L\,j,i} = (y_j + \delta_i \sin \beta_j)/\rho \tag{3.18}$$

where

ϵ_L = longitudinal strain

i = thickness nodal index

j = web width nodal index

ρ = longitudinal radius of curvature.

The corresponding transverse strain is

$$\epsilon_{T\,j,i} = \delta_i / R_t - \bar{\mu}\, \epsilon_{L\,j,i} \tag{3.19}$$

where

ϵ_T = transverse strain

R_t = transverse curvature

$\bar{\mu}$ = inelastic form of Poisson's ratio

and where other symbols have been previously defined.

The relation for the inelastic form of Poisson's ratio is, from Ades (3),

$$\bar{\mu} = \{1 - [(1+d)/(1+e_i)]^{1/2}\}/e_i \tag{3.20}$$

where

e_i = equivalent uniaxial strain

and the relation for d is given by

$$\begin{cases} d = (1+\epsilon_{PL})(1-\mu\,\epsilon_{PL})^2 - 1 \ , & e_i > \epsilon_{PL} \\ \bar{\mu} = \mu \ , & e_i \le \epsilon_{PL} \end{cases} \tag{3.21}$$

where

ϵ_{PL} = strain at the proportional limit

μ = Poisson's ratio.

For the half-flange shown in Figure 5 the equations are similar to those for the web:

$$\delta_i = (i - 1)\, t/4 - t/2 \;, \quad j = 1, 2, \ldots 5 \tag{3.22}$$

$$\epsilon_{L\,j,i} = (y_j + \delta_i \cos \beta_j)/\rho \tag{3.23}$$

$$\epsilon_{T\,j,i} = \delta_i \left(\frac{d^2 w}{d x^2}\right)_j \tag{3.24}$$

where Equations 3.12 through 3.16 are utilized.

Distortion Calculations

The steps in determining the distortion of the cross-section with known strains are as follows:

1. Assume a value the longitudinal curvature

2. Assume a distortion magnitude as given in Equation 3.11.

3. Compute the equivalent uniaxial strain for all nodal points.

4. Use the Ramberg-Osgood (13) three-parameter stress-strain relations:

$$e_i = \sigma_i/E\left[1 + 3/7\,(\sigma_i/\sigma_{0.7})^{n-1}\right] \tag{3.25}$$

$$U = \sigma_i^2/E\left\{0.5 + [3n/7\,(n+1)](\sigma_i/\sigma_{0.7})^{n-1}\right\} \tag{3.26}$$

where

σ_i = equivalent uniaxial stress

e_i = equivalent uniaxial strain

$\sigma_{0.7}$ = Ramberg-Osgood intercept parameter

n = Ramberg-Osgood slope parameter

U = Strain energy density at e_i.

Since U is also the incremental work per unit area for a nodal point, this value must be integrated over the thickness and the perimeter to determine the total work for the cross-section.

5. The total work is obtained in the following relation, using a half-flange as an example:

$$W = \int_A (U_{j,i})\, d\gamma\, ds \tag{3.27}$$

$$\left(\frac{dW}{ds}\right)_j = \left[U_{j,1} + U_{j,5} + 4(U_{j,2} + U_{j,4}) + 2U_{j,3}\right] t/12 \tag{3.28}$$

$$W = \left[\left(\frac{dW}{ds}\right)_1 + \left(\frac{dW}{ds}\right)_5 + 4\left(\frac{dW}{ds}\right)_2 + 4\left(\frac{dW}{ds}\right)_4 + 2\left(\frac{dW}{ds}\right)_3\right] \frac{(b+t)}{24} \tag{3.29}$$

where

W = total work of the half-flange

i = thickness index

s = tube wall width coordinate

γ = tube wall thickness coordinate

j = width index

U = strain energy density

$\frac{dW}{ds}$ = derivitive of work with respect to s

and the numerical process is carried out using Simpson's rule.

This procedure is followed out for the quadrant above the neutral axis and one below. The result is doubled to account for the other symmetrical half.

6. Since the desired value of distortion is that which renders dW a minimum for a given curvature, one must repeat steps 2 through 5 until the distortion affording the minimum work is found.

Finally this process, steps 1 through 6, must be repeated for each value of curvature desired.

Moment Determination

The bending moment of the entire section can be computed in a similar way to that used in determining the internal work. The longitudinal stress is given by

$$\sigma_L = [E_s/(1-\bar{\mu}^2)](\epsilon_L + \bar{\mu}\,\epsilon_T) \tag{3.30}$$

where

E_s = secant modulus (σ_i/e_i)

$\bar{\mu}$ = inelastic form of Poisson's ratio

ϵ_L = longitudinal strain

ϵ_T = transverse strain

and where subscripts defining the nodal points are omitted for simplicity.

The resisting moment is obtained by numerically integrating

$$dM = \sigma_L\, y\, d\gamma\, ds$$

where

M = resisting moment of the cross-section

$d\gamma$ = increment of wall thickness

ds = increment of flange or web width

and Simpson's rule is again used.

Iterative Techniques

Iterative schemes have been devised to accomplish the simultaneous solution of Equations 3.18 through 3.26 which deal with the determination of inelastic stresses from strains. Although the techniques developed are perhaps of interest, the details will not be discussed for sake of brevity. The reader is referred to subroutine "CURVE" in Appendix A where comment cards are included to point out details of the iterative schemes used.

Computations

Appendix B contains the computer program utilized to obtain theoretical results for the distortion theory.

CHAPTER IV

EXPERIMENTAL ANALYSIS

Introduction

A series of pure bending tests was conducted utilizing commercially available mill-formed structural steel tubing of square cross-section. The test specimens ranged in width from two to six inches (outside dimensions), having B/t between 16.5 and 34.5. The initial tests served in part to provide qualitative information on the deformation of the tube cross-section during bending. All of the eighteen tests performed provided quantitative data for use in investigating the validity of the two theoretical approaches. One particular result desired from the test program was an indication of the lowest B/t for which a square tube can still be considered as having a thin-tube flange buckling failure. For lower B/t values, then, the failure would be more of a material nature with accompanying distortions of the cross-section, rather than a buckling one.

Experimental Procedure

Experiments on round steel tubes (3) have indicated that a moment-curvature relation such as that shown in Figure 6 will be typical of the lower B/t specimens in this analysis. Referring to line A in the figure it is seen that there can be two values of curvature associated with a single moment value. If one

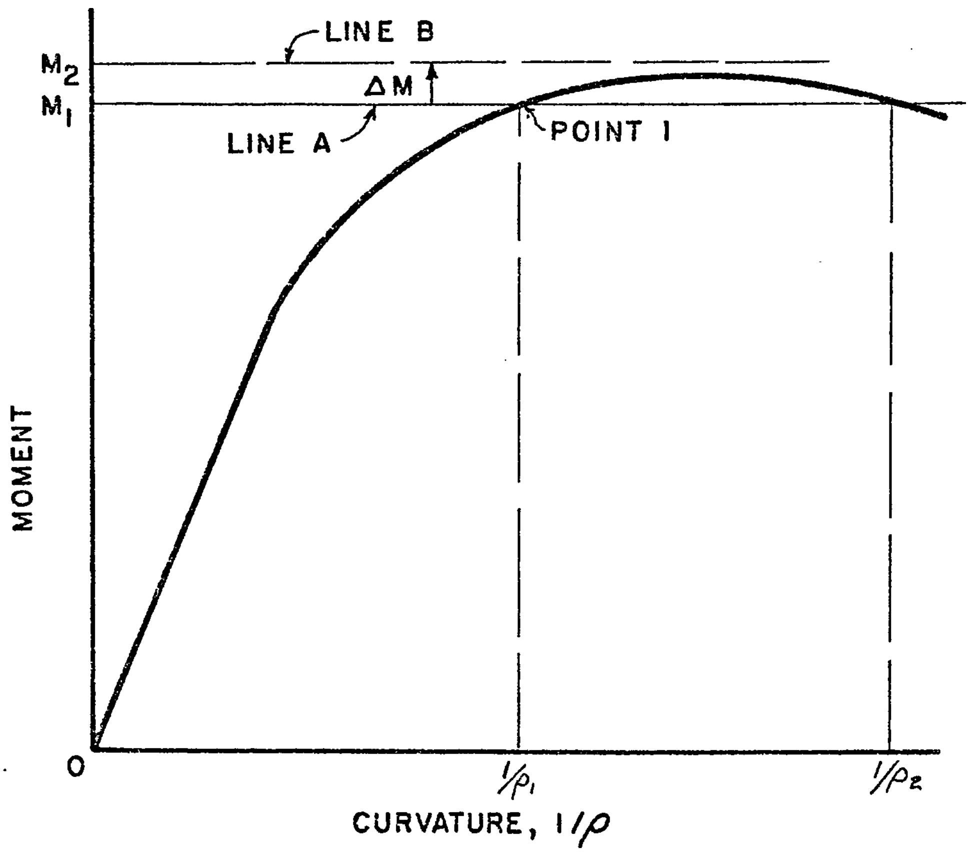

Figure 6. Typical Moment-Curvature Relation for a Low B/t Tube.

were to apply increments of load to determine the maximum moment, one might achieve a condition such as point 1. If, however, an additional load increment were added, such as that indicated by line B, the specimen would rapidly fail in a dynamic manner, giving no opportunity to measure the maximum moment and the corresponding curvature.

In the conduct of these experiments the curvature is then treated as the independent variable and the resisting moment as the dependent variable. Using this controlled-curvature approach the resisting moment will always be single-valued for curvature. The maximum moment as well as the critical curvature at maximum moment can be determined by observing the initial increase, and then the subsequent decrease in resisting moment as the curvature is increased.

Because of the relative flatness of the moment-curvature relation in the inelastic range, one can easily approximate the moment at which yielding of the material occurs using elastic considerations. Using this result, it is expected that one can conservatively predict the highly inelastic maximum moment. Clearly a better indicator of the point at which maximum moment occurs is found in the curvature magnitude, rather than in the moment magnitude. In this investigation at least equal emphasis was placed on curvature as a failure condition indicator.

Dimensionless Parameters

It is convenient to consolidate experimental results in the form of dimensionless numbers. If the forms of the dimensionless quantities are carefully derived utilizing the Buckingham Pi theorem or carefully devised by understanding the nature of the variables involved, one can use them as scaling factors for studying tubes not covered in this analysis. The validity of the dimensionless parameters will become apparent as the diverse range of test data are correlated.

One can make the resisting moment of the tube dimensionless by dividing it by the yield moment. A convenient form of the yield moment is that of Equation 2.10, replacing the ultimate stress by the yield stress (defined as the stress corresponding to a strain of 0.5%). The reason for using the yield stress is that the relatively thin-walled tube will most likely collapse long before stresses in the ultimate range occur. The dimensionless moment expression is then

$$\bar{M} = M / M_{yld} \tag{4.2}$$

where

M = resisting moment at a given curvature

M_{yld} = yield moment based on a 0.5 percent strain value.

A convenient form for the dimensionless curvature is suggested in the work by Timoshenko (2). It will be shown in the results that follow that an expression similar to the square root of λ in Equation 2.5 is a useful dimensionless curvature expression when defined as

$$\bar{C} = B^2 / \rho t \tag{4.3}$$

where

$\bar{C}$ = dimensionless curvature

B = tube outer width

t = tube wall thickness

ρ = longitudinal radius of curvature.

Finally, a convenient form for indicating the amount of distortion of the cross-section in width at the neutral axis is

$$\bar{\Delta} = \Delta B / B \qquad (4.3)$$

where

$\bar{\Delta}$ = dimensionless distortion

ΔB = change in tube width due to distortion

B = tube outer width.

The tube outside width is used as a base for non-dimensional lengths because it is a convenient quantity to measure in practice.

Measurement Techniques

It is evident that measurements of the resisting moment, the applied curvature and the cross-sectional distortion are important. Aside from these parameters, though, the applicability of the flange buckling theory must be examined by measurement of buckling waves on the compressive flange. Also, the assumption of the distortion theory regarding the constant nature of the distortion along the test span at a given curvature must be checked experimentally. Finally, the assumption of a constant radius of curvature over the test span must be confirmed, especially for tubes with lower B/t where the assumption of constant curvature is more suspect. In the paragraphs that follow the techniques that were utilized to obtain the data mentioned above will be described.

Moment Measurement

Conventional tensile load cells were utilized to measure the resisting moment associated with a given increment of curvature. In two of the three bending fixtures utilized it was practically impossible to apply curvatures, because the fixtures were force-controlled rather than deformation-controlled devices. As explanation, a screw-type tensile testing machine is a deformation-controlled device, where a hydraulic-type machine (in which the load is applied directly by a hydraulic cylinder) is a force-controlled device. One can, however, use force controls to continuously adjust the curvature, and with careful control one can, in effect, obtain control of curvature.

Curvature Measurement

The most apparent means of measuring curvature is that of the electric resistance strain gage. The outer fiber strain is measured and the formula

$$1/\rho = 2\epsilon_L/B \qquad (4.4)$$

where

$1/\rho$ = curvature

ϵ_L = measured strain

B = outer tube width

ρ = longitudinal radius of curvature

is used to obtain curvature. Problems which occur experimentally in utilizing the strain gage for this purpose are:

1. If the compressive flange is buckling, the wave will adversely effect the curvature result.

2. If the strains are inelastic and if the strain gages are short, the presence of microscopic slip planes due to yielding will cause an erroneous result.

3. Finally, inherent errors in using strain gages at high strain levels might affect the desired result.

An alternate means for curvature measurement was found in utilizing rigid frames and instrumenting them to read the center deflection with respect to the frame ends. Such a curvature frame is shown in Figure 7. The center deflection is converted into a curvature reading by treating the tube as having a constant curvature, and then fitting the three points formed by the transducer tip and the two ends with a circular arc. The appropriate curvature is

$$1/\rho = \frac{2\delta}{\ell^2} \tag{4.5}$$

where

ρ = radius of curvature

δ = transducer deflection reading

ℓ = half-length of the frame.

Any deflection measuring device, such as a dial gage or a linear potentiometer used here can be utilized as a transducer for the curvature frame. A distinct advantage of using the curvature frame is that the reading so obtained represents an average curvature over the frame length, as contrasted with a point-type result of the strain gage. A disadvantage is that the accuracy of the device is affected when the curvature is not constant along the frame length as has been found to be the case for lower B/t ratios. Both the strain gage and the curvature

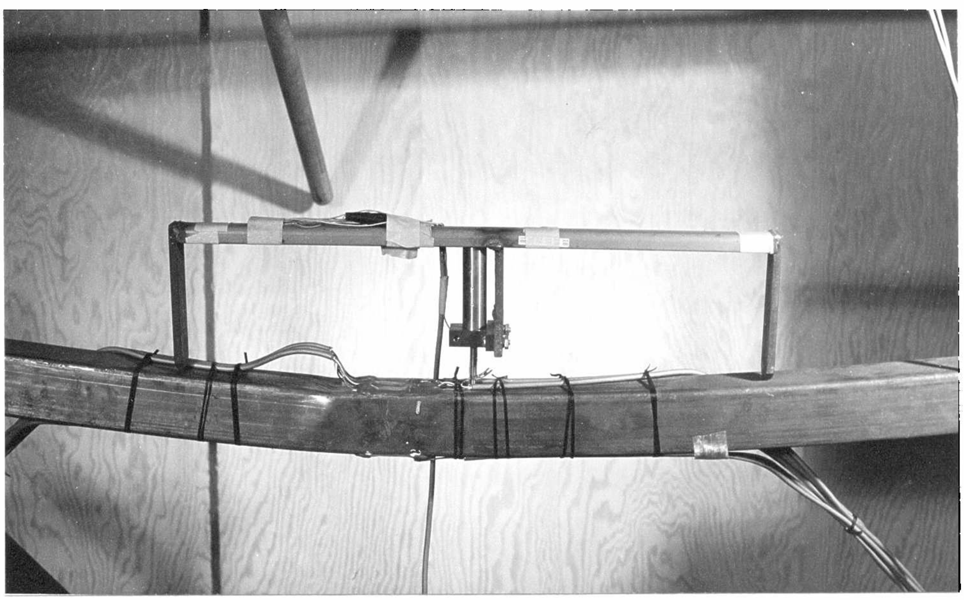

Figure 7. Curvature Measuring Frame.

frame have been utilized for obtaining curvatures in this investigation, and in cases where strain gage pairs and frames are employed on the same test, the results were comparable.

Distortion-Wave Measurement

The change in width of a tube under load, compared with the initial width (measured at the neutral axis) was obtained by using compliance gages as depicted in Figure 8. The compliance gage is, in effect, a flexible "C" clamp, instrumented with a pair of uniaxial strain gages to indicate changes in distance between the tips of the spring-loaded clamp. The clamps, hand-crafted by cold-bending quarter-inch aluminum bars, were calibrated by placing coupons of known thickness between the tube and one end of the clamp and recording the resulting change in strain. The bend radius of the clamp was chosen such that the change in strain caused by a given change in tube width was significant to measure, while avoiding high contact pressures on the tube walls. In some tests compliance gages were used similarly to measure the change in height vertically at the flange centerlines. The results from the vertical measurements were suspect, however, because they indicated the total of the change in height due to the constant distortion as well as a periodic one due to buckling. It is more desirable to measure the total distortion field, but the author was not able to develop a technique for obtaining such field data without an inordinate amount of effort when compared with the scope of this investigation.

A simple means was devised, however, for using a point-type transducer

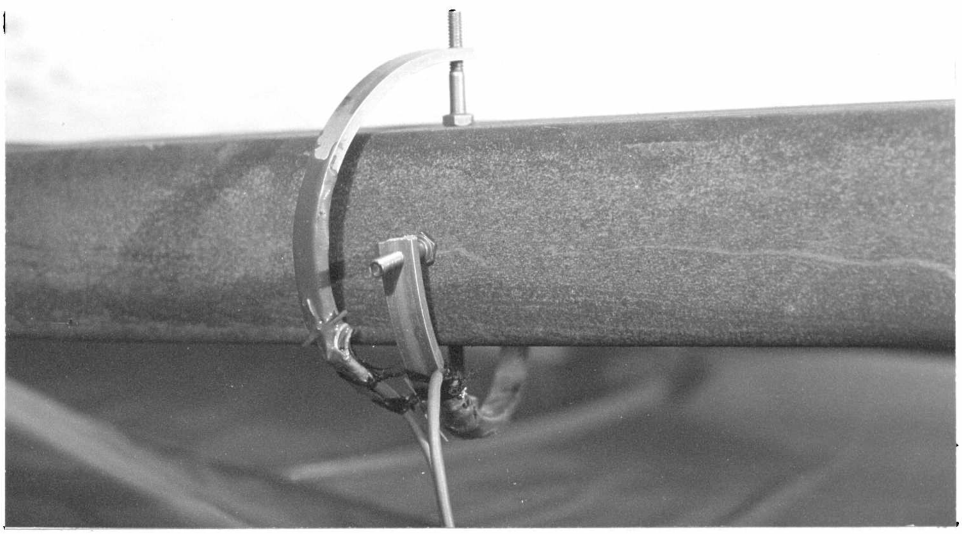

Figure 8. Compliance Gages for Distortion Measurements.

to measure the deflection of the center of the compressive flange with respect to the tube corners as a function of tube span. The device shown in Figure 9 is not unlike the longitudinal curvature measuring frame described previously. The deflection of the flange centerline with respect to the frame ends in contact with the flange corners is measured. An additional feature is that the device is connected by a thin wire to a sheave on a ten-turn rotary potentiometer attached to the base of the bending fixture near one end of the specimen. Using an X-Y recorder, the deflection from the linear potentiometer is placed on the Y-axis, and the distance along the span from the rotary potentiometer is placed on the X-axis. If suitable scaling factors are applied, the resulting plots indicate the relative deflection of the flange centerline as a function of distance along the tube span. This device was found to not only display the buckling wave pattern for the higher B/t, tubes, it also indicated whether the distortion of the compressive flange is constant in the case of the lower B/t tubes.

Test Specimens

All of the square tubing test specimens were standard mill-formed, hot-rolled steel structural tubing. The tubing is actually made from initially round electric-resistance-welded pipe. Since the additional process of squaring the round tube is involved, rectangular tubing is generally more expensive than round pipe. Since the standard length of tubing of this kind is about twenty feet, and since the test specimen length varied between 4 1/2 and 8 feet, several specimens could be cut from one piece of stock. In the specimen descriptions

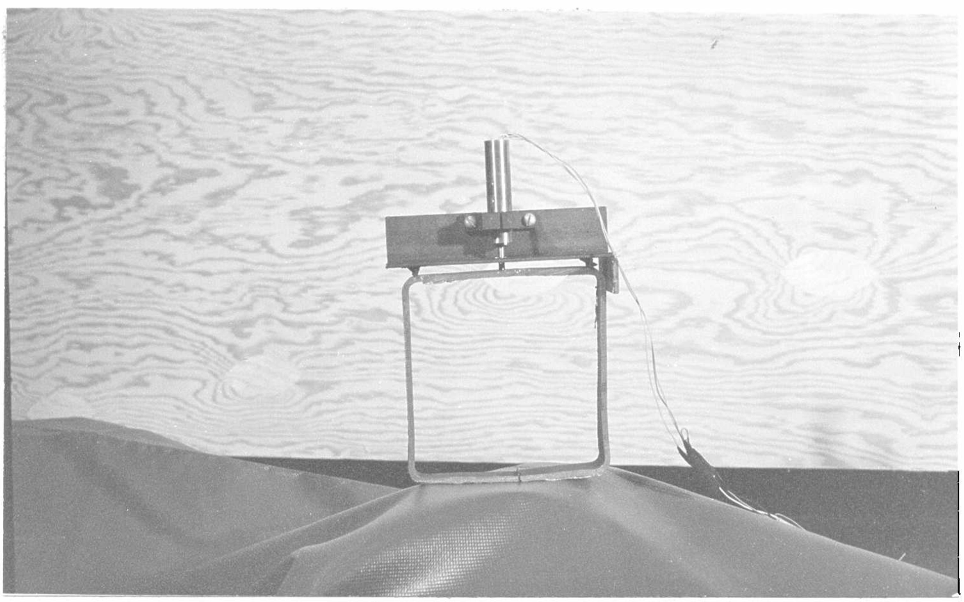

Figure 9. Buckling Wave Measuring Frame.

that follow, pieces cut from the same stock are designated by a letter from A to F, indicating the long-tube stock from which the speciman was cut. It was found desirable to run several tests on specimens from the same group to check repeatability of results.

Table I contains a summary of the specimens utilized in each of the 18 tests on the six specimen groups. Every effort was made to obtain as wide a range of B/t as possible. Although it was possible to obtain lower B/t tubes, it was not experimentally practical to test them. Thicker specimens required load and deformation measurement ranges outside the capability of the instrumentation.

Coupons of the tube specimens were sent to the Shilstone Testing Laboratory of Houston, Texas, for a determination of the stress-strain characteristics of each specimen group. The table also contains yield and ultimate strength properties as well as a description of the types of experimental stress analysis techniques used in each test. Stress-strain data obtained from Shilstone are included as Appendix C.

Bending Fixtures

Three different types of bending fixtures were employed during the test program. The two types used for the two-inch to three-inch specimens are shown in Figure 10. Fixture I, used in tests 1, 2, 3 and 17, was designed to allow the application of a pure bending moment without an accompanying transverse shear at the support or load points. The balancing tensile and compressive loads creating the bending moment act in a direction parallel to the undeformed bending

TABLE I

Square Tube Bending Test Descriptions

Test	B (in)	t (in)	B/t	$\sigma_{.005}$ (psi)	σ_{ult} (psi)	Specimen Group	Type Expts.	Type Fixture
1	2.0	0.062	32.3	44,700	53,500	C	1,2	I
2	2.0	0.121	16.5	57,100	63,600	A	1,2,3	I
3	2.0	0.062	32.3	44,700	53,500	C	1,2	I
4	2.0	0.089	22.3	45,000	49,700	E	2	II
5	2.0	0.089	22.3	45,000	49,700	E	2,3	II
6	2.0	0.089	22.3	45,000	49,700	E	2,3	II
7	2.0	0.089	22.3	45,000	49,700	E	2,3	II
8	2.0	0.121	16.5	57,100	63,600	A	2,3	II
9	2.0	0.062	32.3	44,700	53,500	C	2,3	II
10	2.0	0.121	16.5	57,100	63,600	A	2,3	II
11	2.0	0.121	16.5	57,100	63,600	A	2,3,5	II
12	2.5	0.079	31.6	54,600	62,900	B	2,3	II
13	2.5	0.079	31.6	54,600	62,900	B	2,3	II
14	2.5	0.079	31.6	54,600	62,900	B	2,3	II
15	2.0	0.121	16.5	57,100	63,600	A	2,3	II
16	3.0	0.117	25.6	58,700	69,600	D	2,3	II
17	2.0	0.062	32.3	44,700	53,500	C	4	I
60	6.0	0.174	34.5	57,650	67,050	F	2,4,5	III

Experiment types:

1 strain gages (2)
2 longitudinal curvature frame
3 cross-section distortion collar
4 fully strain-gaged
5 wrinkle measurements using linear potentiometer

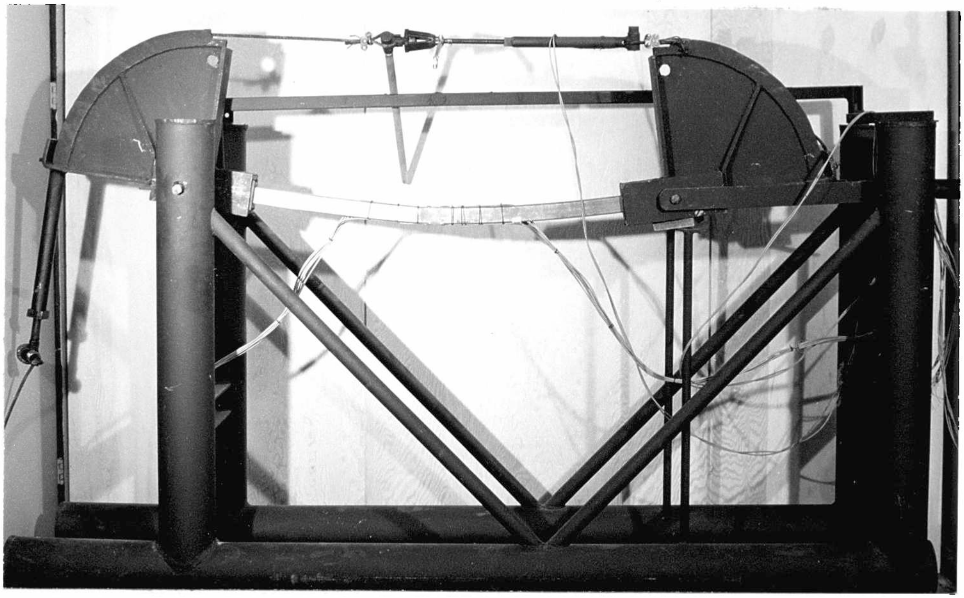

Fixture I

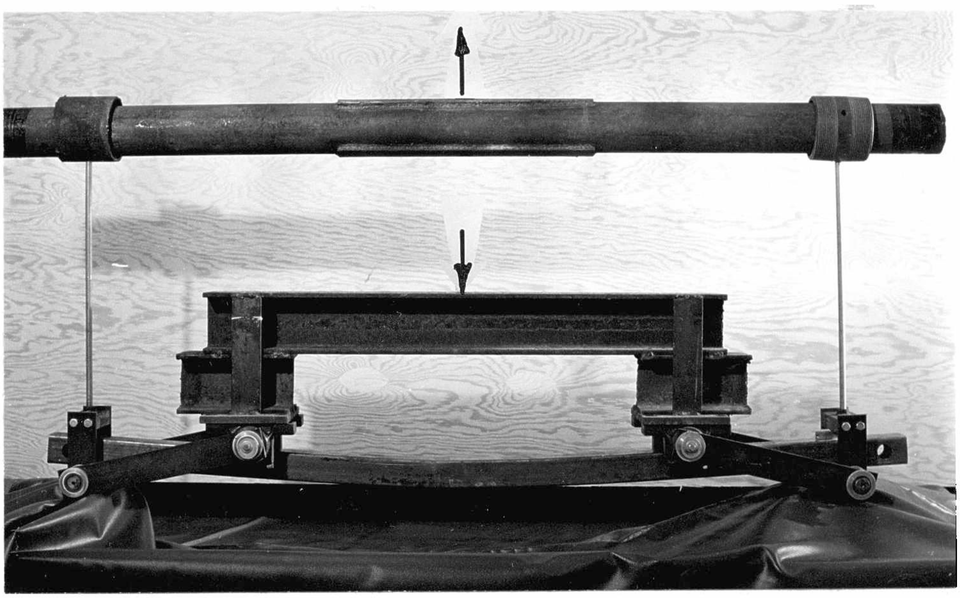

Fixture II

Figure 10. Small Bending Fixtures.

specimens. In using this type of fixture the failure would always occur near the center span of the specimen length. The major disadvantage of using this fixture was found in the load application difficulty. To minimize costs, loads were applied by screwing threaded bars into sockets. The problem was that the experimenter became increasingly exhausted as the test progressed, with the low B/t tubes being the most demanding. Fixture I, however, provided the benefit of having the upper compressive flange exposed for measurements.

Fixture II, shown also in Figure 10, is the standard four-point loading fixture for constant moment determinations. The fixture containing the specimen was placed in an Instron 10,000-pound screw-type testing machine for loading. The disadvantage with this type of frame, especially in cases where buckling is involved, is that there is a high probability of failure near the load application points. As long as stress concentrations were minimized by the use of external pads and internal inserts, however, there was no discernable effect of the fixture on the test results. Tests with this fixture were less demanding than those with the former from a physical standpoint.

Fixture III, shown in Figure 11, was borrowed for use in testing the one large six-inch specimen (Group F) from Shell Development Company. It was designed by the author to test six-inch round pipe specimens. This fixture is of the same basic design as Fixture I, but it is much larger, having a 40,000-pound direct load capacity in testing eight-foot-long specimens.

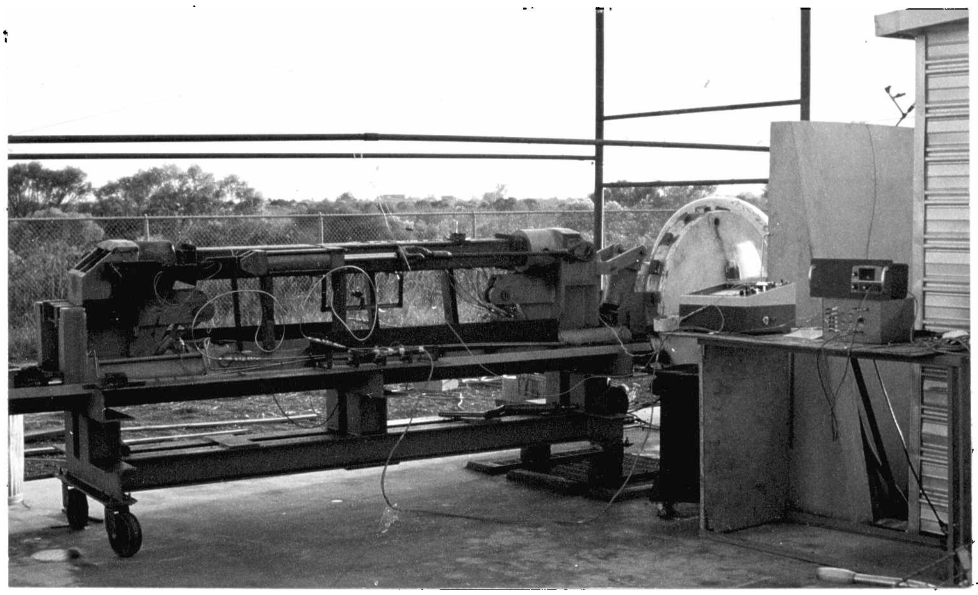

Fixture III

Figure 11. Six-Inch Specimen Bending Fixture.

Instrumentation

In the case of Fixtures I and III, loads were read from the strain-gaged load cells using a Budd Model P-350 Strain Indicator. Load cells were calibrated against a known reference after fabrication and prior to test use. When Fixture II was used, the load cells associated with the Instron testing machine were utilized, as was the built-in load-displacement plotting device. All strain readings were made with a second Budd Indicator, utilizing a switching unit for channel selection. Gages used on the tubing specimens were single Micro-Measurements Type EA-06-500BH-120 uniaxial gages for high strain applications. For the compliance gages two strain gages were active, providing a half-bridge setup. The linear and rotary potentiometers were DC powered using a standard measurement circuit. Readout of the results was accomplished with a Digitec Model 211 digital voltmeter or a Houston Instruments Model HR-96 plotter.

Test Procedure

The test specimens were loaded in increments of curvature, and load, curvature and distortion data were recorded at each increment. Every attempt was made to determine the maximum moment point, along with the corresponding curvature.

CHAPTER V

RESULTS AND CONCLUSIONS

Summarized Results

Dimensionless moment-curvature results from the six specimen groups studied experimentally are presented in Figure 12. The behavior of dimensionless moment as a function of dimensionless curvature and B/t, given in Figure 12, justifies the choice of these parameters.

Dimensionless distortion-curvature results from the experiments, shown in Figure 13, indicate that specimen groups having a B/t of 25 and greater yield a nearly linear relation and are thin-walled, while those having lower B/t values show a nonlinear distortion relation and are thus thick-walled.

The experiments indicate that for the tubes investigated the maximum moment can be approximated by

$$M_{MAX} = 1.15\, M_{yld} \qquad (5.1)$$

where

M_{max} = maximum resisting moment of the cross-section

M_{yld} = yield moment.

and where the expression for the yield moment is given by

$$M_{yld} = \sigma_{.005}\, Bt\left[3B/2 - 3t\right] \qquad (5.2)$$

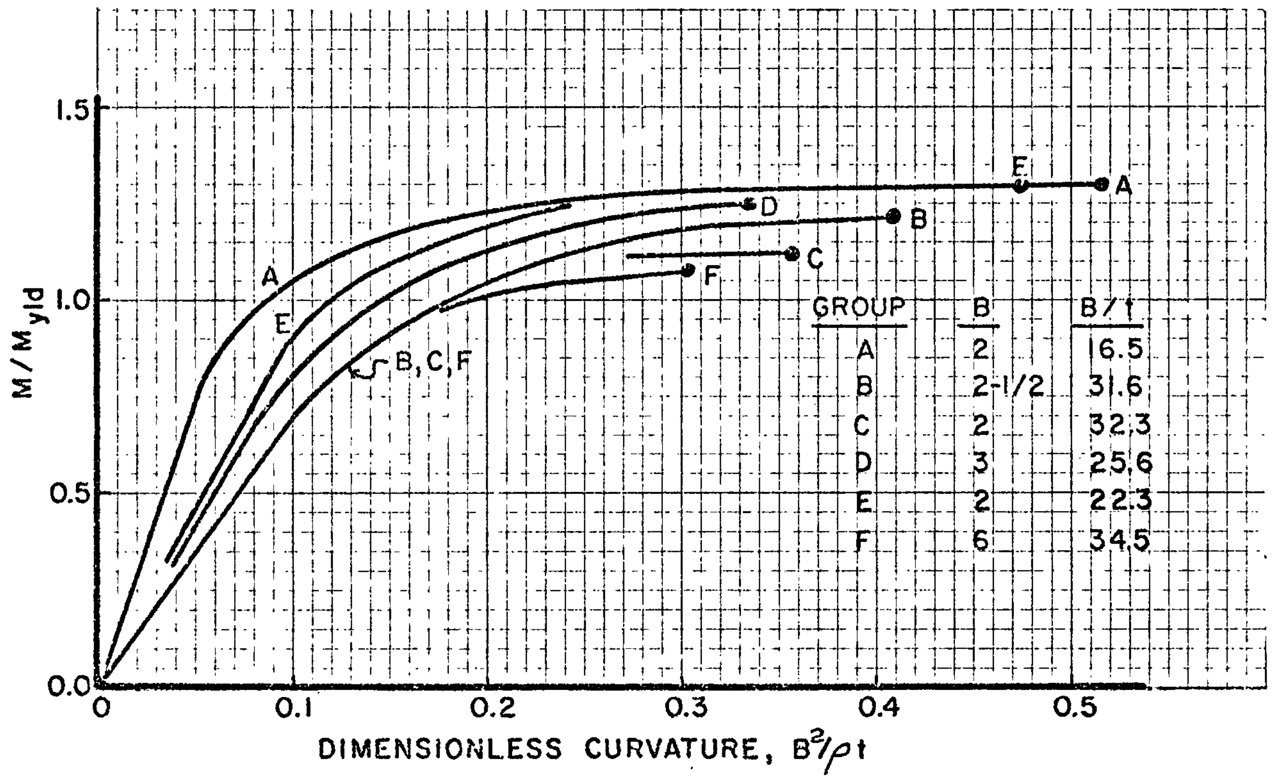

Figure 12. Experimentally Determined Moment-Curvature Relations.

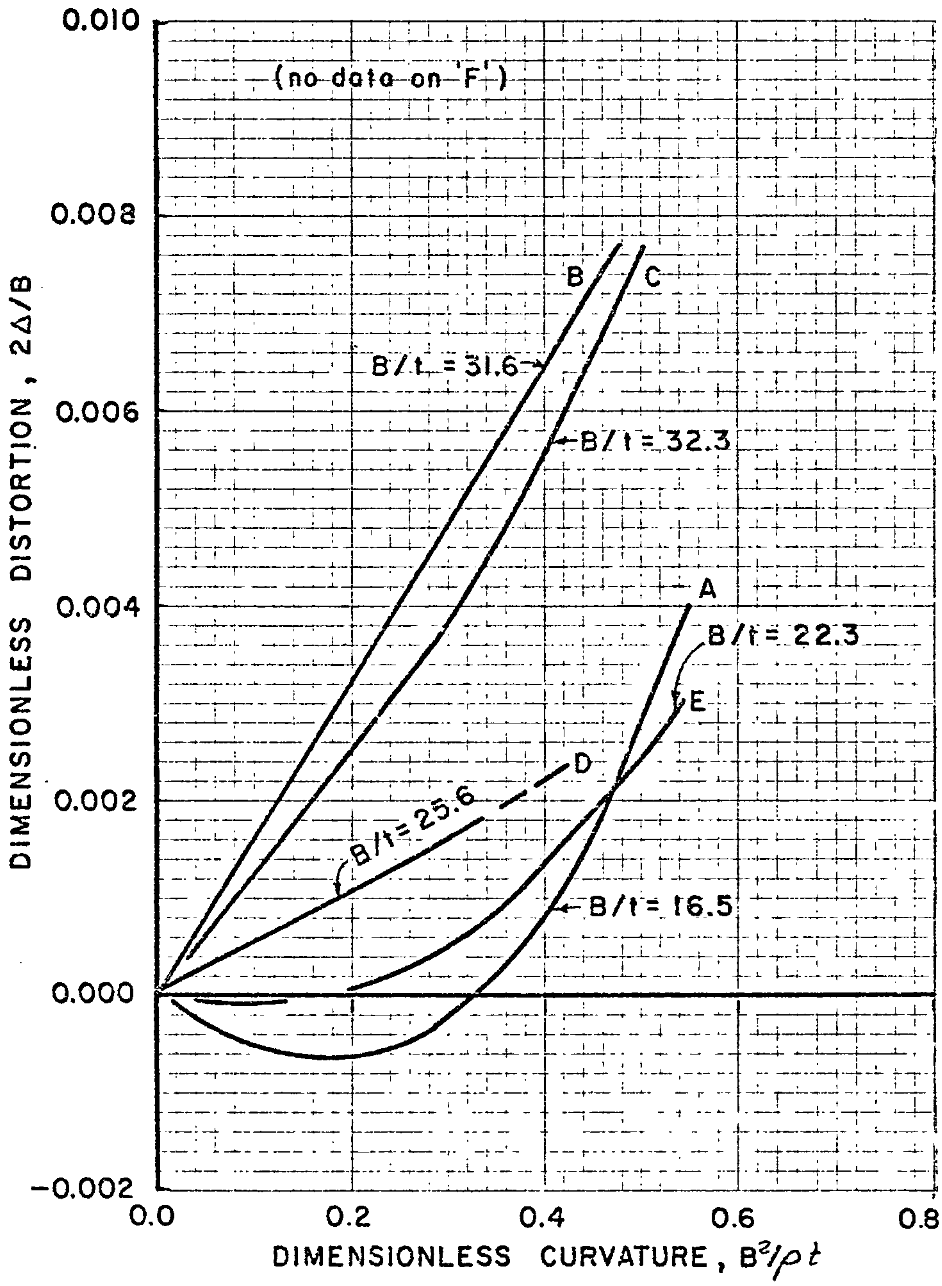

Figure 13. Experimentally Determined Distortion-Curvature Relations.

and

$\sigma_{.005}$ = stress at 0.5% yield strain

B = outer tube width

t = wall thickness.

Similarly the critical curvature can be found by applying the results from these experiments using the dimensionless curvature expression

$$B^2/\rho_{CR}t = 3/8 \qquad (5.3)$$

where

ρ_{CR} = longitudinal radius of curvature at maximum moment.

Both theories, the buckling one and the distortion one, predicted the maximum moment well. Poor agreement is found for the distortion-theory-predicted critical curvatures for all B/t values and good agreement is found for the buckling theory, provided that B/t > 25. Figure 14 contains the critical dimensionless curvature comparisons as a function of B/t for the theories and experiments.

A comparison between the distortion theory and the experiments was seriously affected by residual longitudinal wall bending strains as high as 0.13% found in the tubing. This is apparently more serious in the case of the distortion theory than it is in the buckling theory, as Figure 14 indicates. One specimen group, having a B/t of 31.5, exhibited smaller residual strains than the other ones. As a result, the comparison between the distortion theory and the experiments for that specific specimen group was good.

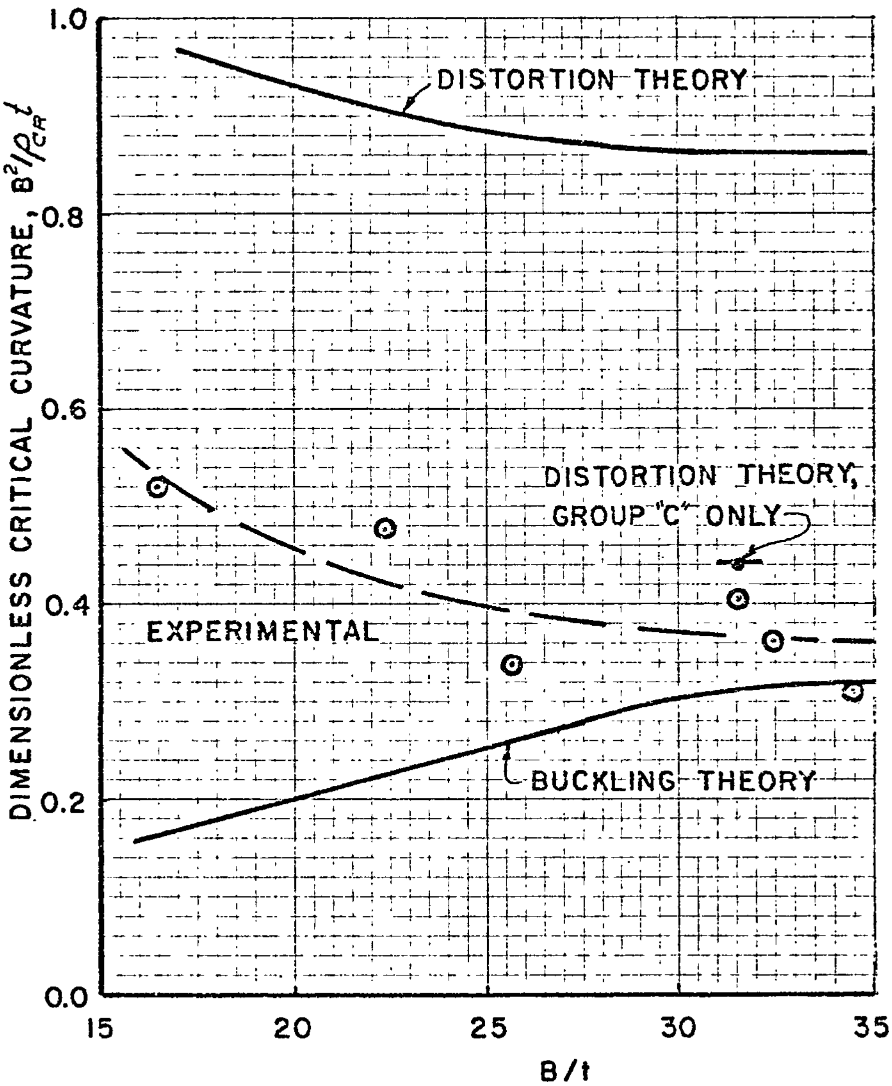

Figure 14. Critical Curvature versus B/t for Experiments and Theories.

Discussion of Experimental Results

The results from the 18 tests are summarized in Table II. Contained in the table are maximum resisting moment and critical curvature. A typical failed specimen is shown in Figure 15.

The results are further consolidated by averaging the results for each specimen group as shown in Table III. Shown for each specimen group (or B/t ratio) are the average moment and curvature as well as the number of tests upon which the average is based. It is seen from this table that all of the results lie within a dimensionless yield moment range of 1.0 to 1.3 and have dimensionless curvature from 0.3 to 0.5.

Moment-Curvature

Figure 12 shows a composite of the moment-curvature relations for each of the specimen groups as determined by experiment. The points of maximum moment and critical curvature are indicated for each specimen group by the dots terminating that curve. It is instructive to note from the curve that:

1. The specimen groups with the steepest elastic slopes are the thickest in terms of the B/t ratio.

2. Nondimensionalizing the moment does not remove all of the scatter in moment magnitudes, although it does limit the range of scatter.

3. The curves for the specimen groups with approximately the same B/t ratio of 32 to 35 are coincident through most of the curvature range. This uniformity is important because the tube widths in this case were 2, 3 and 6

TABLE II

Square Tube Bending Test Results

Test	B	B/t	Specimen Group	M_{max} (ft-lbs)	M_{max}/M_{yld}	M_{max}/M_{ult}	$1/\rho_{CR}$ (1/ft)	$B^2/\rho_{CR} t$
1	2.0	32.3	C	1275	1.14	0.82	0.052	0.28
2	2.0	16.5	A	2775	1.00	0.82	0.180	0.50
3	2.0	32.3	C	1080	0.96	0.69	0.042	0.23
4	2.0	22.3	E	1965	1.26	0.98	0.102	0.38
5	2.0	22.3	E	1984	1.28	0.98	0.156	0.58
6	2.0	22.3	E	2085	1.34	1.03	0.097	0.36
7	2.0	22.3	E	2037	1.31	1.01	0.157	0.58
8	2.0	16.5	A	3441	1.35	1.02	0.235	0.65
9	2.0	32.3	C	1296	1.16	0.83	0.105	0.57
10	2.0	16.5	A	3450	1.35	1.02	0.169	0.46
11	2.0	16.5	A	3274	1.28	0.97	0.194	0.53
12	2.5	31.6	B	3161	1.12	0.87	0.048	0.32
13	2.5	31.6	B	3504	1.24	0.96	0.069	0.45
14	2.5	31.6	B	3547	1.25	0.98	0.070	0.46
15	2.0	16.5	A	3312	1.29	0.98	0.171	0.47
16	3.0	25.6	D	7679	1.26	0.91	0.053	0.34
17	2.0	32.3	C	1095	0.98	0.70	0.066	0.36
60	6.0	34.5	F	40425	1.10	0.82	0.018	0.31

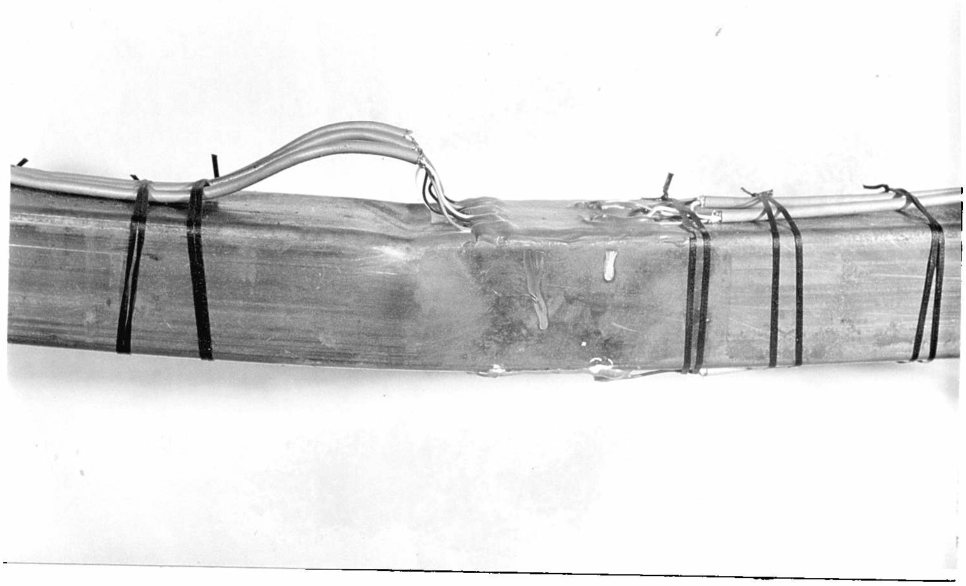

Figure 15. Typical Collapsed Tubing Specimen.

TABLE III

Square Tube Bending Test Summary
By Specimen Group

Specimen Group	B	B/t	M_{max}/M_{yld}	M_{max}/M_{ult}	$B^2/\rho_{CR}t$	No. Tests
A	2	16.5	1.27	0.96	0.52	5
B	2 1/2	31.6	1.20	0.94	0.41	3
C	2	32.3	1.06	0.76	0.36	4
D	3	25.6	1.26	0.91	0.34	1
E	2	22.3	1.30	1.00	0.48	4
F	6	34.5	1.1	0.82	0.31	1

where

B = outer width of tube

t = wall thickness

M_{max} = maximum moment

M_{yld} = yield moment (0.5% strain)

M_{ult} = ultimate moment

ρ_{CR} = critical radius of curvature inches. This one result serves to verify the applicability of the dimensionless curvature expression as an important scaling factor.

The close scatter range of the dimensionless curvature results is appealing from an experimental viewpoint because it is well known that it is difficult to achieve a close scatter band on test results when buckling is the primary failure mode.

Distortion-Curvature

Of equal importance is Figure 13 which is a composite of experimental distortion-curvature relations for each of the specimen groups. Basically the curves show that the sections with higher B/t exhibit a more nearly linear distortion-curvature relation. In the case of Specimen Groups A and E, which have the lower B/t ratios, the curves are quite nonlinear. In fact, the webs were found to deflect inward initially and then finally, at higher curvatures, deflect outward.

It was initially thought that the nonlinear distortion-curvature observations might be an indication of thicker-walled tube behavior. With this reasoning it was tentatively concluded that the lower limit of the thin-walled tube applicability might be at a B/t of about 25. As will be discussed later, it was then learned that residual bending stresses in the tube walls caused by the tube fabrication process might be affecting the results.

A significant result of the data contained in Figure 13 is that for B/t ratios of 25 and above the distortion-curvature relation is approximately linear.

Flange Displacement

Measurements were made of the compressive flange displacement relative to the flange corners as a function of distance along the test span for two different test specimens. In that this analysis was investigative in nature, it was thought that it would be instructive to collect at least one set of data for a thick-walled specimen and one for a thin-walled specimen. Displacement data from Test 11 on Specimen Group A, having B/t of 16.5 are included in Figure 16. Although some wave activity is seen in the shape of the curves, the more prominent effect is that the relative displacement of the compressive flange is far from constant along the test span. This surprising result does not necessarily mean that end effects are likely the cause, since the span length to tube width ratio is twelve. The more likely cause of the nonuniform displacement curve is that the thicker tubes exhibit a non-uniform distortional failure mode along the constant moment span. This same effect was observed by Yao (14), treating relatively thick-walled round pipes subject to pure bending loads. Needless to say, these findings are in direct conflict with the distortion theory of Ades (3), both for round pipes and for square tubes.

Figure 17 contains displacement results from the test of the six-inch specimen test, (Group F), having a B/t ratio of 34.5. The span-width ratio is the same as that of Group A, discussed previously, but in this case there is clearly no sign of end-effect. Furthermore, the failure mode is definitely flange buckling. The half-wave length, averaged along the span, was 5.65 inches. Using von Karman's (5) assumption that the effective width at buckling is the

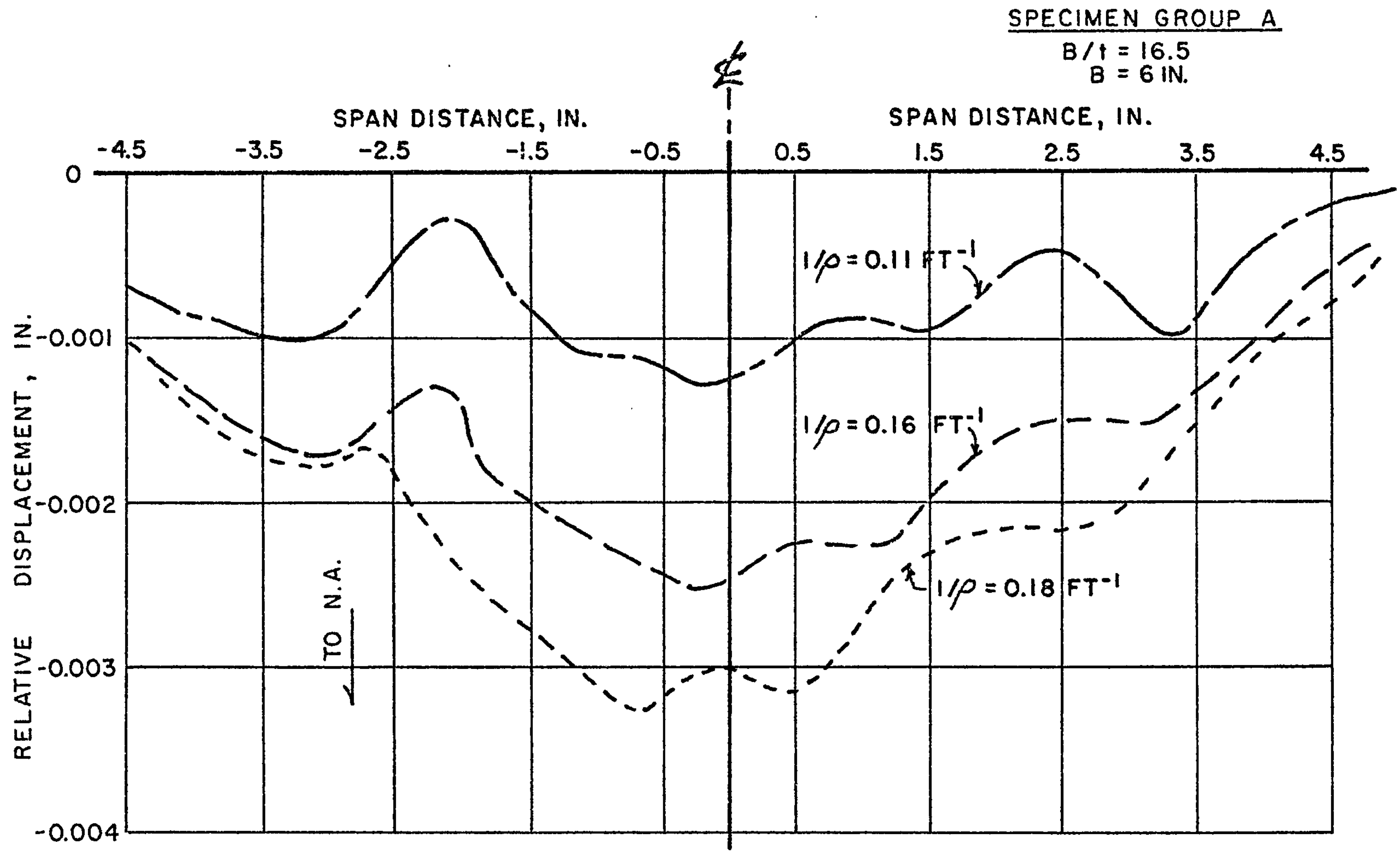

Figure 16. Relative Displacement of Compressive Flange versus Span Length for Specimen Group A, Test 11. Displacement is of the Compressive Flange Centerline Relative to the Flange Edges.

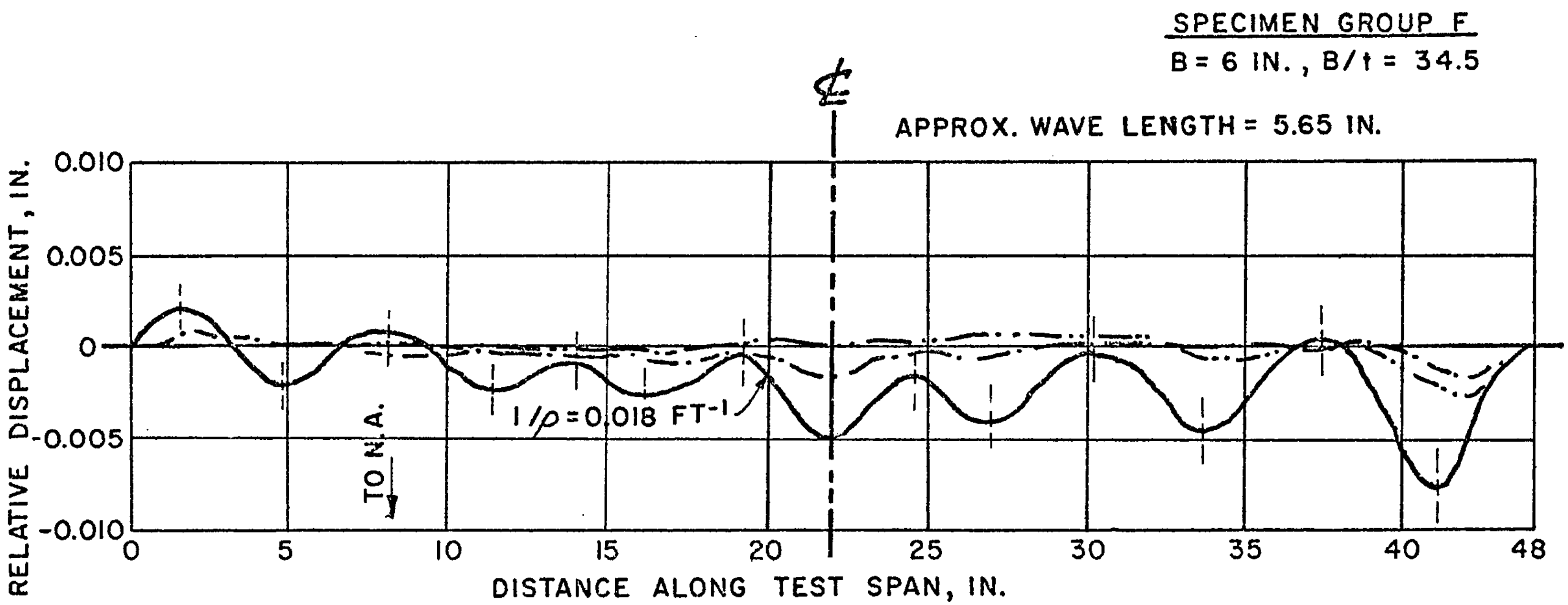

Figure 17. Relative Displacement of Compressive Flange versus Span Length for Specimen Group F, Test No. 60. Displacement is of the Compressive Flange Centerline Relative to the Flange Edges.

half-wave length, this means that the corresponding (total) effective width is 5.65 inches for the 6-inch wide flange.

In summary, Figures 16 and 17 indicate that a change in failure mode from that of inelastic buckling to distortion occurs as the B/t ratio is decreased from 34.5 to 16.5. In the buckling case the compressive flange wave pattern is somewhat uniform along the span length, but in the distortion case the compressive flange relative displacement is clearly not constant with length.

Tube Corner-Strength

It was suggested by the dissertation committee that a possible effect on the experimental-theoretical comparison might be that of the increased strength of the square tube corners caused by the fabrication process. To isolate this effect, tensile coupons were cut from the center of the webs and flanges as well as from the corners of a piece of Specimen Group B having a B/t ratio of 31.6 The results of tensile tests on the side and corner specimens are contained in Table IV. It is seen that the corner specimens, tested with a right angle cross-section and flattened ends, had an average yield strength of 61,750 psi while the center specimens had a yield strength of 54,500 psi, a 13.3 percent increase in strength based on the strength of the sides. Since the corners are only a small percentage of the tube perimeter, it is felt that this effect would not be noticeable within experimental error.

Unlike that done for the bending test stress-strain results, the author prepared the tensile specimens for the corner effect tensile tests, rather than

TABLE IV

Variation of Group B Material Properties Due to Forming
2 1/2" by 0.079" Square Tube

Specimen Taken From:	$\sigma_{.005}$ (psi)	σ_{ult} (psi)
A. Center of Web of Flange		
No. 1	56,200	64,400
No. 2	52,800	63,500
No. 3	54,600	62,900
Average	54,500	63,600
B. Corner of Web-Flange Joint		
No. 1	61,400	69,200
No. 2	62,100	68,900
Average	61,750	69,050

Notes:

1. Stress values are based on a standard tensile test, ASTM A370, except that the widths of the coupon were reduced to 0.5 inches to isolate the corner properties.

2. The corner specimens had an angular test cross-section which was not flattened prior to tensile testing. The grip ends were flattened.

having it done by the outside testing laboratory. It was during the tensile specimen preparation that large longitudinal residual bending strains were found. The wall tensile specimens exhibited a distinct curvature after cutting. Additional tests on this effect were conducted and the results follow.

Residual Forming Strains

After residual forming strains were found, longitudinal strips were cut from each of the specimen groups. The spring-back of the specimen is illustrated in Figure 18. It is seen that when the tube is intact, tensile strains are found on the outer surfaces of the tube and compressive strains on the inner. These effects are summarized in Table V. Web strains were of the same order of magnitude as the flange strains, and the strains adjacent to the welds were slightly larger, on the whole, than those on sides away from the longitudinal weld. Surprisingly, the magnitudes of these tube wall bending strains were quite large compared to the strains at the proportional limits of the materials. In fact, these bending strains must have had an appreciable effect on the tensile stress-strain tests run in conjunction with the bending tests. It is seen from Table V that the residual strains, measured with a curvature frame, approached 0.13% for Specimen Groups D, E, and F. An interesting discovery was that Specimen Group C, having the lowest residual strains, is the same group for which the only flat inelastic stress-strain curve was obtained. Specimen Group C had a Ramberg-Osgood slope parameter of 52, indicating a flat curve, while all of the other specimen groups had slope values of between 15 and 24. The

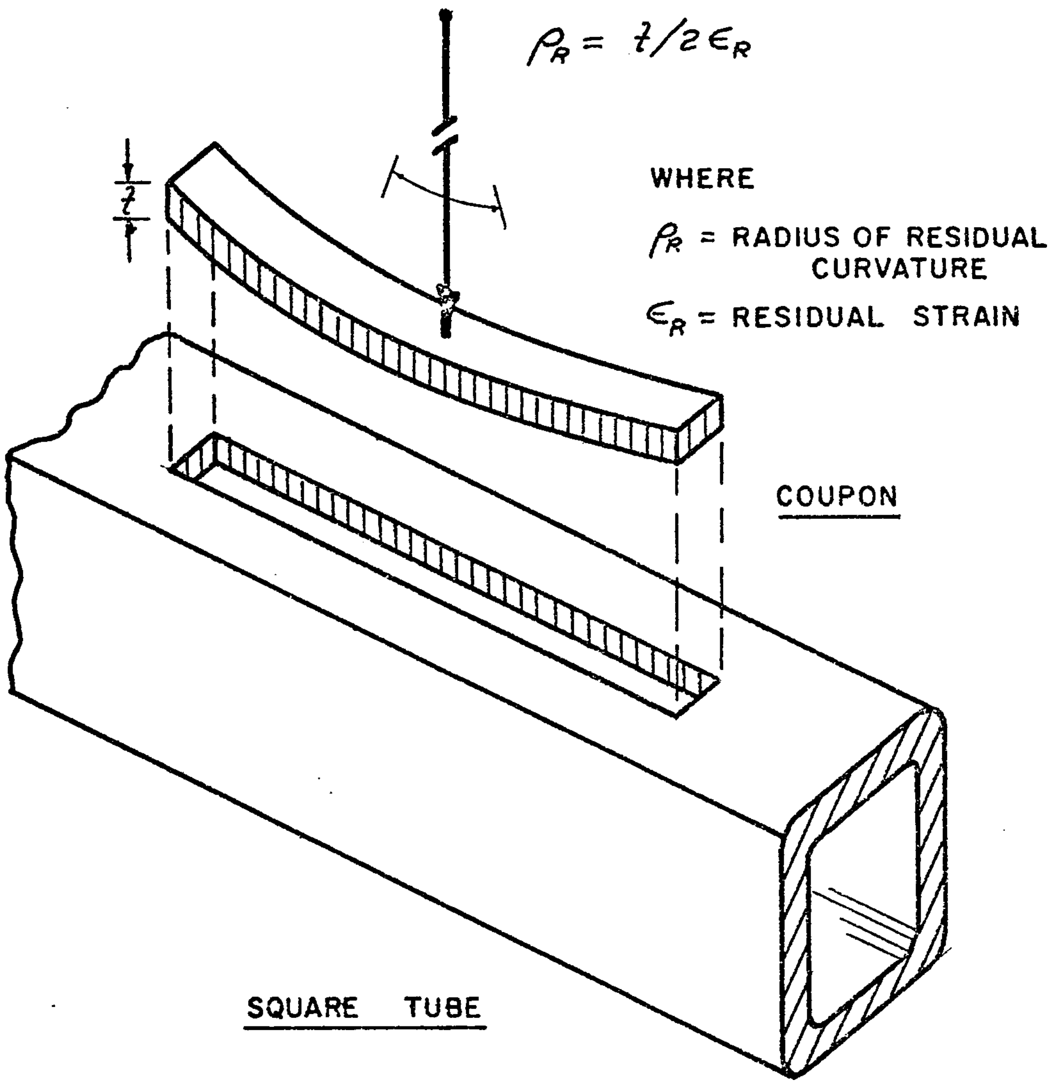

Figure 18. Spring-Back Due to Mill-Forming Residual Strains.

TABLE V

Residual Bending Strains Due to Mill-Forming

Group	Bending Test Nos. (Ref)	B	t	B/t	$\bar{\epsilon}_T$	$\bar{\epsilon}_S$	$\bar{\epsilon}_W$	$\bar{\epsilon}_T/\epsilon_{PL}$
A	2, 8, 10, 11, 15	2	0.121	16.5	874	801	983	1.05
B	12, 13, 14	2 1/2	0.079	31.6	924	861	998	0.96
C	1, 3, 9, 17	2	0.062	32.3	528	469	----	0.45
D	16	3	0.117	25.6	1368	1322	1461	1.52
E	4, 5, 6, 7	2	0.089	22.3	1380	1380	1772	1.53
F	60	6	0.174	34.5	----	1303	1276	1.53

where

B = square tube width, outside to outside, inches

t = tube thickness, inches

$\bar{\epsilon}$ = longitudinal residual bending strain, micro-in.

ϵ_{PL} = strain at proportional limit of the material

and where subscripts are

t = top, or compressive flange of tube

s = side, or web of tube

w = adjacent to the longitudinal tube weld

Ramberg-Osgood parameters for the specimen groups are found with the stress-strain data in Appendix C. The residual strain specimens are shown in Figure 19.

Comparison of Theory and Experiment

A comparison of the maximum moments based on the two theories and the experimentally determined ones in Table VI show very good agreement between the theoretically predicted and the experimentally determined bending moments. The maximum error is found for Specimen Group D, where the local buckling theory is 13 percent lower than the experiment. This confirms the previous observation that it is not difficult to predict the maximum moment of materials having flat inelastic stress-strain curves (see Appendix C).

A comparison of dimensionless curvature values in Figure 14 indicates that for $B/t > 25$, good agreement is obtained between the buckling theory and the experiments. (It is believed that agreement within 25% is acceptable for such buckling results.) Detailed comparisons of significant experimental and theoretical results for each specimen group are included in Appendix D.

Figure 14 also shows that the cross-sectional distortion theory is not useful in determining the critical curvature. It is in error by nearly a factor of two on the high side of the experimental results, except for the single case of Specimen Group C, for which case the residual forming strains were small and for which the stress-strain curve was almost totally flat in the inelastic range.

Based on the data presented concerning Specimen Group C, it is concluded

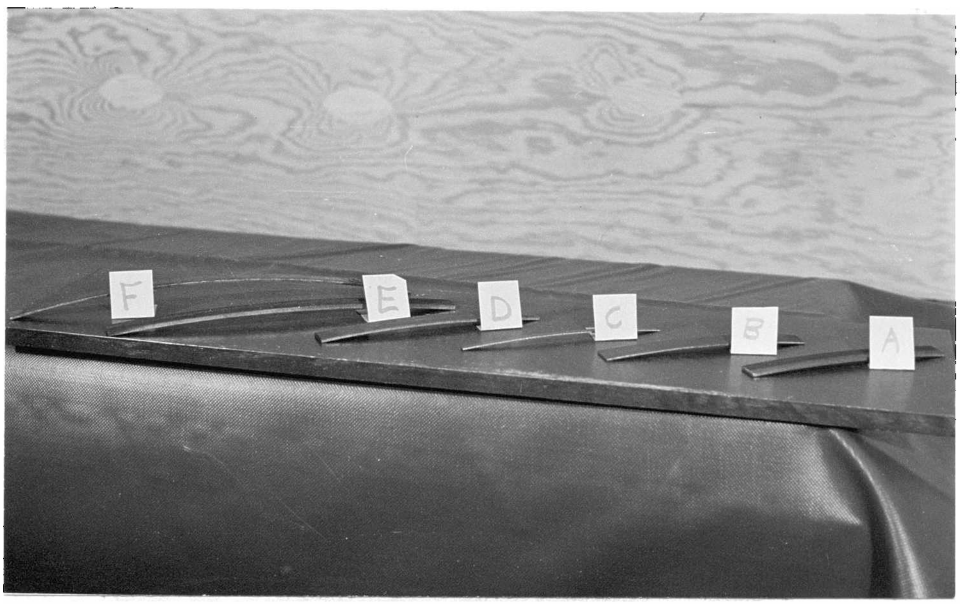

Figure 19. Spring-Back Coupons for All Specimen Groups. Note the Curvature of the Specimens.

TABLE VI

Comparison of Experimental and Theoretical Results

Material	B	B/t	Experiment M_{max} (ft-lbs)	Experiment $B^2/\rho_{CR} t$	Local Buckling M_{max} (ft-lbs)	Local Buckling $B^2/\rho_{CR} t$	Distortion M_{max} (ft-lbs)	Distortion $B^2/\rho_{CR} t$
A	2	16.5	3250.	0.52	2924.	0.17	3305.	0.97
B	2 1/2	31.6	3404.	0.41	3066.	0.33	3174.	0.86
C	2	32.3	1187.	0.36	1263.	0.31	1269.	0.44
D	3	25.6	7679.	0.34	6680.	0.26	7190.	0.82
E	2	22.3	2018.	0.48	1777.	0.22	1841.	0.95
F	6	34.5	40425.	0.31	40030.	0.31	42877.	0.90

that the residual longitudinal bending strains from the mill-forming caused the tubing in the other specimen groups to behave differently from that predicted by the distortion theory. In the sole case of Group C, where the residual strains were lower, reasonable agreement between the distortion theory and the experiments was found. This is apparently more serious in the case of the distortion theory than it is in that of the buckling theory, since the latter compares more favorably with the experimental results.

In summary, there are two possible reasons why the experimental curvature results and the distortion theory results do not agree:

1. The residual strains adversely affect comparison with the theory, as discussed above.

2. The assumption of a constant distortion configuration as a function of length is invalid, particularly for low B/t. The measured low B/t case showed a distinct maximum distortion at the center, decreasing on each side of center span—in direct conflict with the constant curvature assumption.

Conclusions

General

The following conclusions are tendered, based on the results of this square tube bending investigation:

1. The lower bound on the thin-gage behavior of the hot-rolled structural steel square tubing considered in this analysis has been found to be defined by a width-to-thickness ratio, B/t, of 25. Tubing with B/t ratios above this value fail

due to the buckling instability of the compressive flange: tubing with ratios below this value fail due to excessive distortion of the tube cross-section.

2. Residual tube wall bending strains in excess of one tenth of one per cent were measured in some of the tubing tested. These strains, probably caused by the process of squaring round, electric-resistance-welded tubing to make this type of square tubing, should be accounted for in any analysis that is involved with this type of structural tubing.

3. The inelastic flange buckling analysis proposed by Rhodes and Harvey was found to be applicable to the analysis of this type of square tubing, provided that the width-to-thickness parameter, B/t is in excess of 25. The effect of the residual strains was more appreciable in the case of the distortion theory-experiment comparison than it was in the buckling theory-experiment one, because the experimentally determined stress-strain results are also affected.

4. A correlation of the experimental results reveals that the maximum resisting moment of a tube cross-section when subjected to increments of curvature can be approximated by the relation

$$M_{MAX} = 1.15\, M_{yld}$$

where

M_{max} = maximum resisting moment

M_{yld} = yield moment at 0.5% strain.

The critical curvature can be found from the experimentally determined expression

$$B^2/\rho_{CR}\, t = 3/8$$

where

B = tube outside width

t = wall thickness

ρ_{CR} = critical radius of curvature.

Design Implications

Since the AISI design method does not account for inelastic material behavior, this work is of no direct consequence to it. The results, however, might be utilized to extend the AISI specifications to cover inelastic behavior. These results speak clearly for placement of a lower-bound on B/t in the definition of a light-gage structural member. No such limit presently exists because inelasticity is not considered.

This study has shown that as long as hot-rolled structural tubing is fabricated in such a way that appreciable residual longitudinal bending strains are produced, this material should not be included under the AISI light gage steel specification. To include it would require that the specification be altered to account for the residual strains from the tubing squaring process.

Recommendations for Further Studies

An obvious topic for further study is that of including the residual bending strains in the theories and then making comparisons to the results of this investigation, supplemented by additional test data of the type obtained in the experimental part of this investigation. Clearly a new distortion assumption is called for in the case of the distortion theory.

A generalization of this study would be to investigate the behavior of rectangular shapes and other materials such as aluminum.

The results from this investigation will clearly bear consideration in the analysis of hot-rolled structural steel tubing under many different combinations of loads, both as a single member and as components of joint design. Finally, the results herein should provide some basis for investigations of the fatigue properties of square structural tubing.

BIBLIOGRAPHY

BIBLIOGRAPHY

1. von Karman, Th., "Uber die Formanderung dunnwandiger Rohre," Zeit. des Vereines Deutscher Ingenieure, Vol. 55, 1911, pp. 1889-1895.

2. Timoshenko, S., "Bending Stresses in Curved Tubes of Rectangular Cross-Section," ASME Transactions, Vol. 45, 1923, pp. 135-140.

3. Ades, C. S., "Bending Strength of Tubing in the Plastic Range," Journal of Aeronautical Science, Vol. 24, No. 8, August, 1957, pp. 605-610.

4. American Iron and Steel Institute, Light Gage Cold-Formed Steel Design Manual. New York: American Iron and Steel Institute, 1961.

5. von Karman, Th., Sechler, E. E., and Donnell, L. H., "The Strength of Thin Plates in Compression," ASME Transactions, Vol. 54, 1932, pp. 53-57.

6. Winter, G. "Stress Distribution in an Equivalent Width of Flanges of Wide, Thin-Wall Steel Beams," NACA Technical Note No. 784, 1940.

7. Cozzone, F. P., "Bending Strength in the Plastic Range," Journal of the Aeronautical Sciences, Vol. 10, No. 5, May, 1943, pp. 137-151.

8. Rhodes, J. and Harvey, J. M., "Alternative Approach to Light-Gage Beam Design," Journal of the Structural Division, ASCE, Vol. 97, No. ST8, August, 1971, pp. 2119-2135.

9. Rhodes, J., "The Nonlinear Behavior of Thin-Walled Beams Subjected to Pure Moment Loading," Thesis presented to the University of Strathclyde at Glascow, Scotland, in partial fulfillment of the requirements for the degree of Doctor of Philosophy, 1969.

10. Steele, M. C., "The Plastic Bending and Twisting of Square Section Members," Journal of the Mechanics and Physics of Solids, Vol. 8, 1954, pp. 156-166.

11. Dwyer, T. J., and Galambos, T. V., "Plastic Behavior of Tubular Beam Columns," Journal of the Structural Division, ASCE, Vol. 91, No. ST4, August, 1965, pp. 153-168.

12. Smith, T. R. G., "The Post-Buckled Behavior of a Thin-Walled Box Beam in Pure Bending," International Journal of Mechanical Science, Vol. 14, 1972, pp. 711-722.

13. Ramberg, W., and Osgood, W. R., "Description of Stress-Strain Curves by Three Parameters," NACA Technical Note No. 902, July, 1943.

14. Yao, J. C., "Large-Deflection Analysis of Buckling of a Cylinder Under Bending," Journal of Applied Mechanics, Transactions of the ASME, Vol. 29, No. 4, December, 1962.

APPENDICES

APPENDIX A

Computer Program for Buckling Analysis

BUCKLING THEORY COMPUTER PROGRAM

Written in Fortran V for the Univac 1108, Exec II

```
C
C      SQUARE TUBE BENDING ANALYSIS  BASED ON THE
C      FLANGE BUCKLING APPROACH OF RHODES AND HARVEY
C
C      RAY R. AYERS,     C.E. DEPARTMENT,  UNIVERSITY OF HOUSTON
C      DR. JAMES M. NASH, ADVISOR
C
       DIMENSION   Y(10) ,  YT(10), YS(10), DMTS(10), DMTT(10),
      1  DMCS(10)
       COMMON RO, SMAX, SPL, RN, S07, E           ,AMU
C      NNJJ = THE NUMBER OF DIFFERENT SQUARE TUBE CASSES TO BE RUN
       READ(5,1111)     NNJJ
 1111  FORMAT (I5)
       DO 88     JJJI = 1, NNJJ
       READ(5,100)   H, T, E , AMU, RN, S07, SPL ,  SMAX ,SYLD,EYLD
C
C      H = SQUARE TUBE WIDTH, CENTERLINE DIMENSIONS  , INCHES
C      T = TUBE WALL THICKNESS, INCHES
C      E = MODULUS OF ELASTICITY, PSI
C      AMU = POISSONS RATIO, ELASTIC FORM
C      RN = RAMBERG OSGOOD SLOPE PARAMETER
C      S07 = RAMBERG OSGOOD STRESS INTERCEPT PARAMETER, PSI
C      SMAX =  UPPER STRESS LIMIT FOR STRESS ITERATIONS, PSI
C      SYLD = YIELD STRESS AT A STRAIN OF .005, PSI
C      EYLD = YIELD STRAIN CORRESPONDING TO SYLD, IN/IN
C
  100  FORMAT  (  8F10.0      / 8F10.0  )
       READ (5,400)  ROH , ROL       ,XN
```

```
C
C     ROH  = HIGH LIMIT ON RADIUS OF CURVATURE, INCHES
C     ROL = LOW LIMIT ON RADIUS OF CURVATURE, INCHES
C     XN = NUMBER OF  CALCULATIONS BETWEEN ROL AND ROH
C
  400 FORMAT(  8F10.0)
      WRITE (6, 912 )
  912  FORMAT( 1H1      )
      WRITE  ( 6,111 )
  111 FORMAT( 1H1,11X, 'AN ANALYSIS OF THE BENDING CHARACTERISTICS'
     1  // 6X, 'OF SQUARE STRUCTURAL TUBING USING THE RHODES  APPROACH'
     2    ///       )
      WRITE (6,222 )  H
  222 FORMAT(1H0 ,   12X, 'MEAN WIDTH OF SQ. TUBE' , 5X, F10.4,
     1 2X,    'INCHES'     )
      WRITE(6,333 )  T
  333 FORMAT( 1H0, 12X, 'AVERAGE WALL THICKNESS' , 5X, F10.4, 2X,
     1  'INCHES'            )
      WRITE(6,444)   E, AMU
  444 FORMAT(1H0, 12X, 'MATERIAL PROPERTIES' , // 17X,  'ELASTIC '
     1 ,'MODULUS'  , 5X, E10.3, 2X, 'PSI'  // 17X ,
     2 'POISSONS RATIO'  , 5X, F7.3           )
      WRITE (6,666)  SPL, SYLD, SMAX
  666 FORMAT(1H0, 16X,     'STRESS AT PROPORTIONAL LIMIT', 2X, F10.0,
     1  2X, 'PSI'  , //17X, 'YIELD STRESS'  , 5X, F10.0, 2X, 'PSI'  //
     3  17X,  'ULTIMATE STRESS'  , 5X, F10.0, 2X, 'PSI'     )
      WRITE(6, 555)   S07, RN
  555 FORMAT(  1H0, 12X, 'RAMBERG-OSGOOD PARAMETERS'  //
     2 17X, 'STRESS AT MOD. OF 097*E     ', F10.0 //
     3  17X, 'SHAPE FACTOR FOR STRESS-STRAIN FIT' , 5X, F10.2     )
      ROT = (H+T)/2.*E/SPL
      IF(ROH.GE.ROT)   ROH = ROT
      IF(ROH .LE. 1. )   ROH = ROT
      WRITE(6,777)  ROH, ROL, XN
```

```
  777 FORMAT(1HO,///4X,'THIS RUN EXPLORES THE RADIUS RANGE BETWEEN'
     1  //  7X, F10.0, 2X, 'INCHES AND'    , F10.0,   2X,
     2  'INCHES IN'   F10.2, '  INCREMENTS'        )
      EPL = SPL/E
      ET1 = 0.
      DR  =(ROH-ROL)        / XN
      NN = XN
      DO 88  J = 1,NN
      XJ = J
      IF ( XJ  . LE.  0.  )      XJ = 0.
    1  RO = ROH         - DR          *XJ
C     BOTTOM PLATE    CRIPPLING ANALYSIS
C     RO IS THE RADIUS OF CURVATURE FOR WHICH CALCULATIONS ARE DESIRED
      WRITE( 6,456 )  RO
  456 FORMAT(1HO, '**********************' //5X,'MOMENT CALCULATIONS'
     1    , ' FOR RADIUS OF CURVATURE OF' ,  F10.0,2X, 'INCHES' //
     2  '*******************'        )
      I = 0
      YC =-H/2.
      EL = YC/RO
      ET1 = 0.
      EECR = 4.8*E*(T/H)**2         /E
      IF(EECR.LE.EYLD)  ECR = -EECR
      IF(EYLD.LT. EECR)   ECR = -EYLD
      IF(EL.GE.ECR)   GO TO 25
C      EFFECTIVE WIDTH CALCULATIONS
      WRITE(6,911)
  911 FORMAT(1HO, /// 7X, 'THE COMPRESSIVE FLANGE EXCEEDS '
     1 ,'CRIPPLING LIMIT'  // 7X,  'EFFECTIVE WIDTH CALCULATIONS',
     2  ' ARE IN ORDER'          )
  205 CONTINUE
C     HE IS THE EFFECTIVE WIDTH OF THE COMPRESSIVE FLANGE
    9 HE = (0.7*ECR/EL + .3 )*H
      IF( HE.GE. H  )   HE = H
```

```
      SA   = 3.*H*T + HE*T
      SAY = 2.*H**2*T
      YBAR  =  SAY/SA
      DD = - H/2.   + YBAR
      YC = -1.*(H/2.   + DD    )
      EL = YC/RO
      ET1 = 0.
      YQ= YC
      CALL CURVE( EL, ES, 0., ET1, YQ    ,ET, POIS )
      SIGI = ES*(EL   + POIS*ET)/(1. - POIS**2 )
      IF(SIGI + SYLD)  30,30,96
   30 WRITE(6,31 )  SIGI, SYLD
   31 FORMAT(1H0, 'FLANGE YIELD EXCEEDED ' , 2F10.0)
   96 DM = SIGI*YC*T*HE
      WRITE (6, 913)  SIGI, EL,   DD, YC, HE
  913 FORMAT(1H0,10X, 'STRESS  ' , F10.0,  2X, 'STRAIN  ', F10.5, //
     3 11X, 'N. A. SHIFT TO TENS. ',F10.4, //11X, 'FIBER DIST. TO '
     4 ,      'FLANGE C. L.  ' F10.4//11X,'EFFECTIVE WIDTH, CL TO CL'
     5  2X, F10.4                        )
      WRITE(6,814  )
      GO TO 18
   25 CONTINUE
      WRITE( 6, 814 )
  814 FORMAT( 1H0,  /// 2X, 'ELEMENT   L. STRESS    L. STRAIN    '
     2  , 'T. STRAIN    FIBER DIST. '     /)
      DM =     SIGI*YC*T*H
      DD = 0.
C     CALCULATIONS FOR THE TENSILE WEB
   18 DO 5                 I = 1,9
      XI = I
      Y(I) =  (XI - 1. )/8.*H/2.    -DD
      EL = Y(I) / RO
      ET1 = 0.
      CALL CURVE( EL, ES, 0., ET1, Y(I), ET, POIS )
```

```
      SIGI = ES*(EL   + POIS*ET)/(1. - POIS**2 )
      DMTS(I) = SIGI*Y(I)
    5 CONTINUE
C     CALCULATIONS FOR THE TENSILE FLANGE
       DO 7  I = 1,5
      XI = I
      YT(I) = H/2. + (XI-1.)*T/4. - T/2.        -DD
      EL   = YT(I) / RO
      ET1 = 0.
      CALL CURVE( EL, ES, 0., ET1, YT(I),ET, POIS )
      SIGI = ES*(EL   + POIS*ET)/(1. - POIS**2 )
      DMTT(I) =       SIGI*YT(I)
    7 CONTINUE
C     CALCULATIONS FOR THE COMPRESSIVE WEB
      DO 10  I = 1,9
      XI = I
      YS(I)    = - (XI  - 1.)/8. *H/2.     -DD
      EL = YS(I)/RO
      ET1 = 0.
      CALL CURVE( EL, ES, 0., ET1, YS(I),ET, POIS )
      SIGI = ES*(EL   + POIS*ET)/(1. - POIS**2 )
      IF(SIGI+SYLD )  8, 19,19
    8 WRITE(6,32)   SIGI, SYLD
   32 FORMAT(1H0, 'WEB    YIELD EXCEEDED ' , 2F10.0)
   19 DMCS(I) = SIGI*YS(I)
   10           CONTINUE
C    TOTAL MOMENT CALCULATION
      XMTS = DMTS  (1)   + DMTS(9)
      XMTS = XMTS+ 4.*(DMTS(2) + DMTS(4) + DMTS(6) + DMTS(8))
      XMTS = XMTS + 2.*( DMTS(3) + DMTS(5)  + DMTS(7) )
      XMTS  =  XMTS*T*H/8./3.
      XMTT = DMTT(1)   + DMTT(5)
      XMTT = XMTT + 4.*( DMTT(2) + DMTT(4))
      XMTT = XMTT + 2.*(DMTT(3))
```

```
      XMTT = XMTT *H*T/4./3.
      XMCS = DMCS(1)   + DMCS(9)
      XMCS = XMCS + 4.*(DMCS(2)  + DMCS(4)  + DMCS(6)  + DMCS(8))
      XMCS = XMCS + 2.*(DMCS(3) + DMCS(5) + DMCS(7)  )
      XMCS = XMCS *T*H/8./3.
      TM = DM + XMTS + XMTT + XMCS
      TM = TM/12.
      XRO = 1./RO*12.
      WRITE (6,667)             TM,XRO
  667 FORMAT( 1H0, //// 10X, 'MOMENT OF RESISTANCE   ' , E10.4,
     3 '  FOOT*POUNDS'  // 10X,  'FOR A CURVATURE (1/RO) OF'
     5  , '      ',  F10.6,  '  1/FEET'          )
   88 CONTINUE
      END
```

SUBROUTINE "CURVE"

Used in the Buckling and in the Distortion Theories

```
C
C     SUBROUTINE CURVE IS USED TO CALCULATE THE NODAL
C     STRESSES ONCE THE STRAIN IS KNOWN.  THIS SUBROUTINE IS
C     USED BY BOTH THE BUCKLING AND THE DISTORTION THEORIES.
C
C     RAY R. AYERS    CIVIL ENGINEERING DEPARTMENT  UNIVERSITY OF HOUSTON
C     DR. JAMES M. NASH , ADVISOR
C
      SUBROUTINE CURVE(EL, ES, AREA, ET1, Y, ETT,POIS)
      COMMON RO, SMAX, SPL, RN, S07, E          ,AMU
C     EI = THE EQUIVALENT UNIAXIAL   STRAIN         IN/IN
C     EL = LONGITUDINAL STRAIN AT A NODE, IN/IN
C     ES = THE SECANT MODULUS    PSI
C     AREA IS THE AREA UNDER THE STRESS STRAIN CURVE AT EI
C     ET1 = THE DISTORTION COMPONENT OF TRANSVERSE STRAIN. THE
C     POISSON EFFECT IS ADDED IN THE SUBROUTINE
C     Y =  THE 'Y' COORDINATE OF THE NODE
C     ETT = THE TOTAL TRANSVERSE STRAIN CALCULATED IN THE SUBROUTINE
C     POIS = THE VARIABLE POISSONS RATIO, ENELASTIC FORM
C
      IF( RO.LE. 0.   )  Y = 0.
C  UPPER AND LOWER LIMITS ON EI ARE CALCULATED USING THE
C     ELASTIC PROPORTIONAL LIMIT AS ONE BOUND (ES= E),
C     AND USING TOTAL PLASTICITY ( POIS = 0.5) AS THE OTHER
      EPL= SPL/E
      DEL = (1.+EPL)*(1.- AMU*EPL)**2 - 1.
      ETT = ET1 - AMU*Y/RO
       EIL = EL**2+ ETT**2 + 2.        *AMU*EL*ETT
      EIL = (EIL/(1.- AMU**2))       **0.5
      IF(EIL .LE. EPL)          GO TO 25
```

```
       ETT = ET1 - Y/RO /2.
      EIP = EL**2 + ETT**2 + EL*ETT
      EIP = (EIP/.75 )**0.5
      EIHI = EIP
      EILO = EPL
C EI IS FOUND BY ITERATION TO STATEMENT 30
      EI = (  EILO + EIHI   )/2.
   20 POIS = (1. - ((1.+ DEL)/(1.+ EI))**0.5)/EI
       ETT = ET1 - POIS *Y/RO
      EIC = EL**2 + ETT**2 + 2.*POIS*EL*ETT
      EIC = (EIC/(1. - POIS**2))**0.5
      B = (EIC - EI          )
      C = ABS(B)
      IF   (  C . LT.   .000001)   GO TO 30
  300 FORMAT(1X , 8E10.5  )
      IF(EIC - EI )  105, 105, 110
  105 A = EIHI - EI
      B = EIC - EILO
      IF( A . LT. B )  EILO = EILO + B
      IF(  B . LT. A )  EIHI = EIHI - A
      GO TO 115
  110 B = EIHI - EIC
      A = EI - EILO
      IF(A. GT. B)   EILO = EILO + A
      IF(  B . GT. A   )  EIHI = EIHI - B
  115 CONTINUE
      EI = (EIHI + EILO)/2.
      GO TO 20
C     STATEMENT 25 IS THE THE ELASTIC BRANCH, WHERE ITERATION IS NOT
C     NEEDED
   25 POIS = AMU
      EI = EIL
   30 CONTINUE
C  SIG1 AND AREA UNDER CURVE ARE DETERMINED
C        BY TRIAL USING EI KNOWN TO STATEMENT  40
C     FOLLOWING  ARE CALCULATIONS OF THE ITERATION LIMITS
```

```
      IF( EI .LE. EPL )      SIGI = E*EI
      IF( EI .LE. EPL ).  AREA = SIGI *EI/2.
      IF( EI .LE. EPL )     ES = SIGI /EI
      IF( EI .LE. EPL )          GO TO 40
       SHI = SMAX
      SLO = SPL
      SIGI = S07
C     NOW THE ITERATION BEGINS
   33 EIC = SIGI*(1.+ 3./7.*(SIGI/S07)**(RN- 1. ))/E
      B = ( EIC - EI     )
      C =  ABS(B)
      IF ( C . LE. .000001)  GO TO 37
      IF (  B .GT. 0.)  SHI = SIGI
      IF (        B .LE.  0.)    SLO = SIGI
      SIGI = (   SHI + SLO ) / 2.
      GO TO 33
   37  AREA = .5   +( 3.*RN/7./(RN+ 1.))*(SIGI/S07)**(RN - 1.)
      AREA = AREA * SIGI**2/E
      ES = SIGI / EI
   40 CONTINUE
  555 FORMAT(  1X, 10E10.5)
      RETURN
      END
```

APPENDIX B

Computer Program for Distortion Analysis

DISTORTION THEORY COMPUTER PROGRAM

Written in Fortran V for the Univac 1108, Exec II

```
C
C
C      SQUARE TUBE BENDING ANALYSIS BASED ON THE
C      DISTORTION OF THE CROSS - SECTION  METHOD OF ADES
C
C      RAY R. AYERS    CIVIL ENGINEERING DEPARTMENT
C      UNIVERSITY OF HOUSTON
C      DR. JAMES M. NASH , ADVISOR
C
       DIMENSION  BETV(10), YV(10), BETH(10), YH(10),  ELV(10,10)
     1   ,ETV(10,10),                      SIGV(10,10), AV(10,10),
     2    ELH(10,10), ETH(10,10),                SIGH(10,10), AH(10,10)
     3 ,                        DMV(10), DMH(10          ),
     4                   DWV(10),     TW(2) ,         DWH(10)      , TM(2)
     5   , SYH(10) , SYV(10)
       COMMON  RO, SMAX, SPL, RN, S07, E              , AMU
       PI = 3.14159
C      NNJJ = NUMBER OF DIFFERENT SQUARE TUBE CASES
       READ(5, 3010)          NNJJ
 3010  FORMAT(I5          )
       DO 216     JJJJ = 1, NNJJ
       READ(5,100)    H, T, E , AMU, RN, S07, SPL ,   SMAX
     1   , SYLD, XXXX, RR
C
C      H = SQUARE TUBE WIDTH, CENTERLINE DIMENSIONS  , INCHES
C      T = TUBE WALL THICKNESS, INCHES
C      E = MODULUS OF ELASTICITY, PSI
C      AMU = POISSONS RATIO, ELASTIC FORM
C      RN = RAMBERG OSGOOD SLOPE PARAMETER
C      S07 = RAMBERG OSGOOD STRESS INTERCEPT PARAMETER, PSI
```

```
C      SMAX =  UPPER STRESS LIMIT FOR STRESS ITERATIONS, PSI
C      SYLD = YIELD STRESS AT A STRAIN OF .005, PSI
C      EYLD = YIELD STRAIN CORRESPONDING TO SYLD, IN/IN
C      XXXX = DUMMY VARIABLE            DISREGARD
C      RR = RESIDUAL BENDING STRAIN     TO BE ADDED TO PROGRAM
C      AT A LATER DATE
C
  100 FORMAT  (  8F10.0       / 8F10.0  )
      READ (5,400)  ROH , ROL       ,XN ,     ALH       , ALL
C
C      ROH  = HIGH LIMIT ON RADIUS OF CURVATURE, INCHES
C      ROL = LOW LIMIT ON RADIUS OF CURVATURE, INCHES
C      XN = NUMBER OF  CALCULATIONS BETWEEN ROL AND ROH
C      ALH = HIGHEST DISTORTION MAGNITUDE EXPECTED.      THIS  IS
C      THE INWARD DEFLECTION OF THE CENTER OF THE COMPRESSIVE FLANGE, IN.
C      LOWEST  DISTORTION MAGNITUDE DEPECTED. MUST BE .GT. ZERO . IN INCHES
C
  400 FORMAT(  8F10.0)
      WRITE (6, 912 )
  912  FORMAT( 1H1     )
      WRITE  ( 6,111 )
  111 FORMAT( 1H1,11X, 'AN ANALYSIS OF THE BENDING CHARACTERISTICS'
     1  // 6X, 'OF SQUARE STRUCTURAL TUBING USING THE  ADES   APPROACH'
     2    ///       )
      WRITE (6,222 )  H
  222 FORMAT(1H0 ,   12X, 'MEAN WIDTH OF SQ. TUBE' , 5X, F10.4,
     1 2X,    'INCHES'     )
      WRITE(6,333 )  T
  333 FORMAT( 1H0, 12X, 'AVERAGE WALL THICKNESS' , 5X, F10.4, 2X,
     1  'INCHES'           )
      WRITE(6,444)   E, AMU
  444 FORMAT(1H0, 12X, 'MATERIAL PROPERTIES' , // 17X,  'ELASTIC '
     1 ,'MODULUS'   , 5X, E10.3, 2X, 'PSI'  // 17X ,
     2 'POISSONS RATIO'   , 5X, F7.3          )
      WRITE (6,666)  SPL, SYLD, SMAX
  666 FORMAT(1H0, 16X,     'STRESS AT PROPORTIONAL LIMIT', 2X, F10.0,
```

```
     1  2X, 'PSI'  , //17X, 'YIELD STRESS'  , 5X, F10.0, 2X, 'PSI'  //
     3  17X,  'ULTIMATE STRESS'  , 5X, F10.0, 2X, 'PSI'     )
      WRITE(6, 555)   S07, RN
  555 FORMAT(  1HO, 12X, 'RAMBERG-OSGOOD PARAMETERS'  //
     2 17X, 'STRESS AT MOD. OF 097*E      ', F10.0 //
     3  17X, 'SHAPE FACTOR FOR STRESS-STRAIN FIT' , 5X, F10.2    )
      ROT = (H+T)/2.*E/SPL
      IF(ROH.GE.ROT)   ROH = ROT
      IF(ROH .LE. 1. )   ROH = ROT
      WRITE(6,777)  ROH, ROL, XN
  777 FORMAT(1HO,///4X,'THIS RUN EXPLORES THE RADIUS RANGE BETWEEN'
     1  //  7X, F10.0, 2X, 'INCHES AND'   , F10.0,   2X,
     2  'INCHES IN'   F10.2, '  INCREMENTS'      )
      D = (ROH- ROL)
      XXN = XN
C     RO IS THE RADIUS OF CURVATURE FOR WHICH CALCULATIONS ARE DESIRED
      RO = ROH         + D/XXN
      NN = XN
      KJJ = NN + 1
      DO 216  KJ = 1,KJJ
    2 RO = RO  -D/XXN
      WAL = 0.
      WRITE( 6,456 )  RO
  456 FORMAT(1HO, '*********************' //5X,'MOMENT CALCULATIONS'
     1    , ' FOR RADIUS OF CURVATURE OF' ,  F10.0,2X, 'INCHES' //
     2  '********************'       )
    3 ALT = (ALH-ALL)/10.
C     WAL CORRESPONDS TO THE VALUE OF 'W' , WHICH IS TIMOSHENKO'S
C     SQUARE TUBE DISTORTION RELATION
      WAL  = ALL-ALT
    8 CONTINUE
      DO 215  KJK = 1,11
    6 WAL =WAL + ALT
C     THIS DO LOOP ON K ALLOWS CALCULATIONS TO BE MADE
C     FOR THE COMPRESSIVE FLANGE AND WEB, AND THEN TO REPEAT (K=2)
C     FOR THE TENSILE FLANGE AND WEB.  K IS USED TO CHANGE SIGNS
```

```
C      ON THE EQUATIONS WHEREVER THEY CHANGE  BETWEEN THE UPPER
C      AND LOWER HALVES OF THE TUBE
       DO 203   K = 1,2
       TW(K) = 0.
       TM(K) = 0.
       ARG = PI*(H+ T/2.)/(H+T)
       DWX= -WAL*(COS(ARG) + SIN(2.*ARG)/PI)*PI/(H+T)      /1.3183
C      DWX IS DW/DX, THE FLANGE SLOPE AT THE FLANGE- WEB JOINT
C      RT = THE TRANSVERSE WEB RADIUS OF CURVATURE DUE TO DISTORTION
       RT = H/2./DWX
C      THIS DO LOOP IS USED TO CALCULATE THE 'Y' COORDINATES OF
C      THE NODES FOR THE HALF WEB AND HALF FLANGE
C      THE FINAL LETTER OF  'V', OR 'H', ON ANY VARIABLE REFERS
C      TO THE 'VERTICAL' (WEB) OR THE HORIZONTAL (FLANGE).
C      TO THE 'VERTICAL' (WEB) OR THE' HORIZONTAL'(FLANGE).
     7 DO 10  N= 1,5
       XN = N
       BETV(N)= (XN-1.)*(H-T)/8. /RT
       IF(WAL.LE. .00001  )   BETV(N) = 0.
       YV(N) = RT*SIN(BETV(N) )
       IF(WAL.LE. .00001 ) YV(N) = (XN-1.)*(H-T)/8.*(-1.)**(K+1 )
       XX = (H+T)/2.   + (XN-1.)*(H+T)/8.
       ARGG = PI*XX/(H+T)
       BETH(N)= -PI*WAL/(H+T)*(COS(ARGG)+ SIN(2.*ARGG)/PI)/1.3183
       WX = WAL *(SIN(ARGG)+ (1.- COS(2.*ARGG))/2./PI) /1.3183
       YH(N) = (RT*SIN(DWX) - WX   )*(-1.)**(K+1)
       IF(WAL.LE. .00001)  YH(N) =       H/2.          *(-1.)**(K+1)
    10 CONTINUE
  1010 FORMAT( 1H0, ///1H0, 'VERTICAL ELEMENT STRESS AND STRAIN'//
      1  1H0, 3X, 'NODE   '  , 3X, 'THK ELEM' , 3X, 'L STRESS' 3X,
      2   'L STRAIN' , 3X, 'T STRAIN' ///)
C      WEB (VERTICAL) STRAINS AND STRESSES ARE CALCULATED WITH
C      THIS DO LOOP
       DO 20 N = 1,5
       DO 20 I = 1,5
       XI = I
```

```
      DEL = (XI-1.)*T/4.    - T/2.
      ELV(N,I)= (YV(N)+ DEL*SIN(BETV(N)))/RO
      YVNS  = ELV(N,I) * RO
      IF(RR.LE.0. )  GO TO 702
      ELV(N,I) = ELV(N,I) + (DEL/RR)*(-1.)**(K+1 )
  702 ET = (DEL /RT)*(-1.)**(K+1)
      IF(WAL .LE. .00001 )   ET = 0.
      CALL CURVE(  ELV(N,I),  ES, AV(N,I), ET,   YVNS , ETV(N,I),POIS)
      SIGV(N,I)= ES*(ELV(N,I)+POIS*ETV(N,I))/(1. - POIS**2)
 1005 FORMAT( 1H0, 2I10,F10.0 , 2F10.6        )
   20 CONTINUE
 6010 FORMAT( 1H0, ///1H0, 'HORIZ.   ELEMENT STRESS AND STRAIN'//
     1  1H0, 3X, 'NODE    '   , 3X, 'THK ELEM' , 3X, 'L STRESS' 3X,
     2   'L STRAIN' , 3X, 'T STRAIN' ///)
C     FLANGE ,
C     FLANGE ( HORIZONTAL)  STRAINS AND STRESSES ARE CALCULATED
C     WITH THIS DO LOOP
      DO 60 N= 1,5
      DO 60  I = 1,5
      XI = I
      DEL = (XI-1.)*T/4.   -T/2.
      ELH(N,I) = (YH(N) + DEL*COS(BETH(N)))/RO
      YHNS = ELH(N,I)*RO
      IF(RR.LE.0.  )  GO TO 701
      ELH(N,I) = ELH(N,I) + (DEL/RR)*(-1.)**(K+1)
  701 XX = (H+T)/2.   + (XI-1.)*(H+T)/8.
      ARH = PI*XX/(H+T)
      D2W = PI*WAL/(H+T)**2*(2.*COS(2.*ARH) - PI*SIN(ARH)) /1.3183
      ET = DEL*D2W*(-1.)**K
      CALL CURVE(  ELH(N,I),  ES, AH(N,I), ET, YHNS , ETH(N,I), POIS)
      SIGH(N,I)= ES*(ELH(N,I)+POIS*ETH(N,I))/(1. - POIS**2)
 6005 FORMAT( 1H0, 2I10,F10.0 , 2F10.6        )
   60 CONTINUE
C     THIS DO LOOP IS USED TO CALCULATE THE  TOTAL MOMENT (TM)
C     AND THE TOTAL WORK (TW) OF THE SECTION
      DO 607  N = 1,5
```

```
      DO 606 I = 1,5
      SYV(I) = SIGV(N,I)*RO *ELV(N,I)
  606 SYH(I) = SIGH(N,I)*RO *ELH(N,I)
      DMV(N) = SYV(1)+    SYV(5)+4.*(SYV(2)+SYV(4))+  2.*SYV(3)
      DMV(N) = DMV(N)*T/4./3.
      DMH(N)=SYH(1)+    SYH(5)+ 4.*(SYH(2)+SYH(4)) +2.*SYH(3)
      DMH(N) = DMH(N)*T/4./3.
      DWV(N) = AV(N,1)+AV(N,5)+4.*(AV(N,2)+AV(N,4)) +2.*AV(N,3)
       DWV(N) = DWV(N)*T/4./3.
      DWH(N)= AH(N,1) +AH(N,5)  + 4.*(AH(N,2) +AH(N,4)) +2.*AH(N,3)
  607 DWH(N) = DWH(N)*T/4./3.
      XMV= DMV(1) +DMV(5) + 4.*(DMV(2)+DMV(4)) +2.*DMV(3)
      XMV = XMV*(H-T)/8.        /3.
      XMH = DMH(1)+DMH(5) + 4.*(DMH(2)+ DMH(4)  ) +2.*DMH(3)
      XMH = XMH*(H+T)/8. /3.
      WH = DWH(1) + DWH(5) +4.*(DWH(2) +DWH(4)) +2.*DWH(3)
      WH = WH *(H+T)/8.   /3.
      WV = DWV(1) + DWV(5)  + 4.*(DWV(2) + DWV(4)) + 2.*DWV(3)
      WV = WV*(H-T)/8.        /3.
      TW(K) = WV       + WH + TW(1)
      TM(K) =  XMV       + XMH +TM(1)
  203 CONTINUE
C     THE FACTOR OF TWO  ADDS THE CONTRIBUTION OF THE
C     OTHER HALF DUE TO SYMMETRY PERPINDICULAR TO THE N. A.
        TW(2) = TW(2)*2.
        TM(2) = TM(2)*2.         /12.
   15 XRO = 1./RO*12.
      WRITE(6,500)   TW(2) , TM(2) ,WAL ,XRO
  500 FORMAT(1H0,   '  W, XM,WAL, RO   ',     E15.8,5E10.5 )
  215 CONTINUE
  216 CONTINUE
   69 END
```

APPENDIX C

Stress-Strain Data

STRESS-STRAIN RESULTS

Tensile Tests

Coupons from all of the specimen groups were tensile tested in accordance with ASTM Standard A370. Stress-strain curves were recorded, as reproduced in Figure C-1.

Ramberg-Osgood Curve Fit

Experimentally determined stress-strain results were subjected to curve fitting using the Ramberg-Osgood expression listed in Equation 3.25. The results from the curve fitting process, the stress intercept parameter, $\sigma_{0.7}$, and the slope parameter, n, shown in Figure C-1 were used to describe analytically the stress-strain curves, as required in the theoretical approaches.

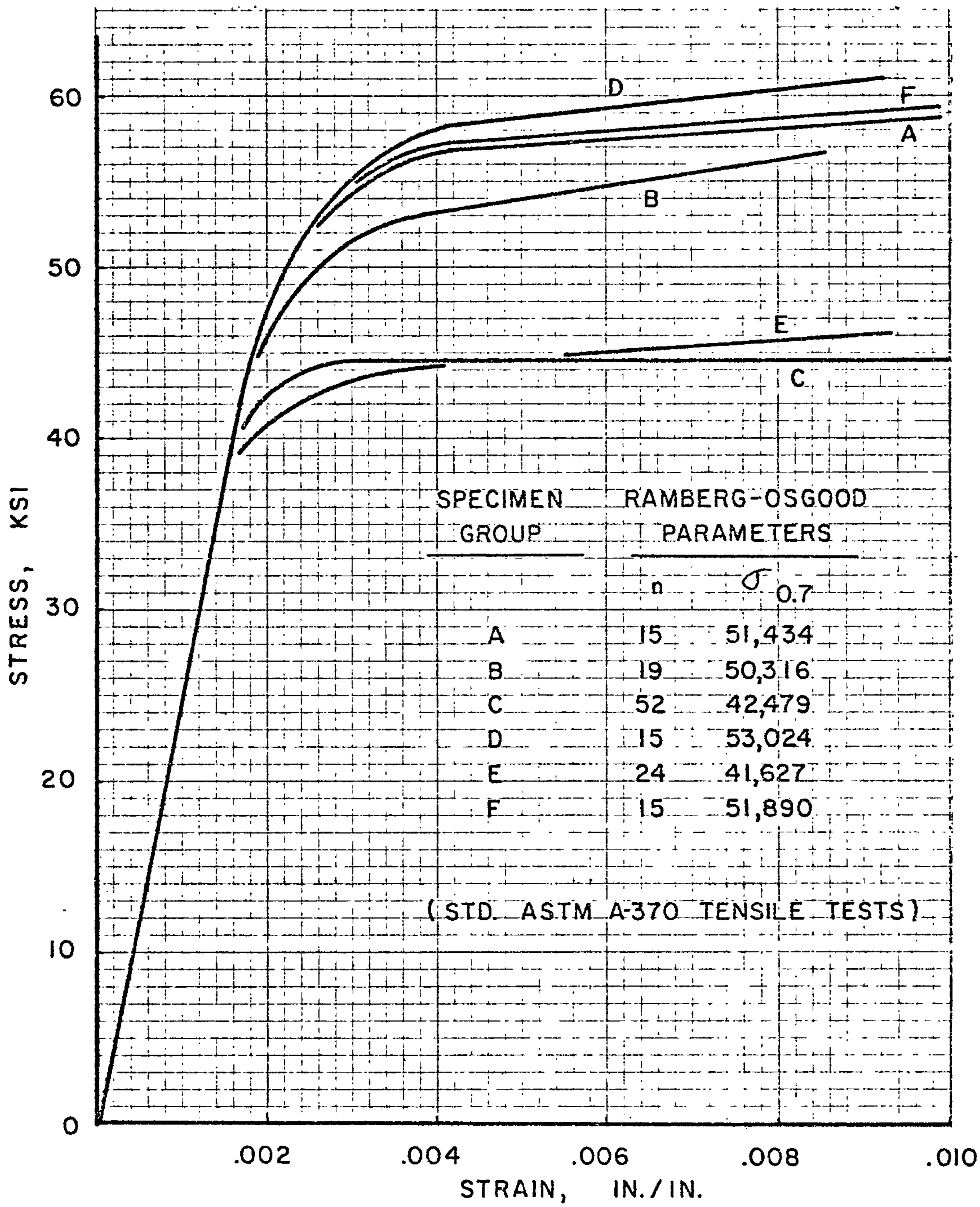

Figure C-1. Stress-Strain Curves for All Specimen Groups.

APPENDIX D

Detailed Comparisons of Experiment with Theories

1. Moment-Curvature Curves

2. Distortion-Curvature Curves
   (Experiment only)

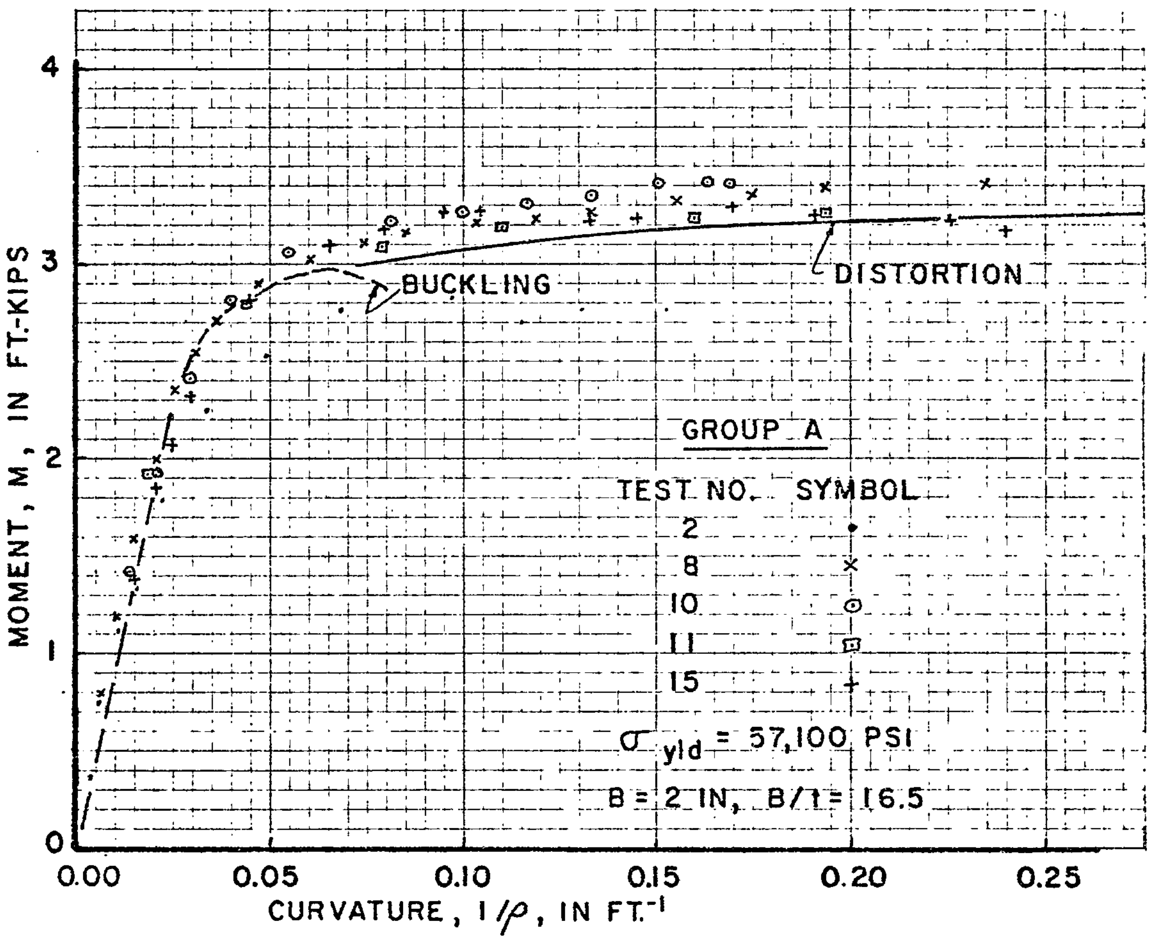

Figure D-1. Moment-Curvature Plots for Specimen Group A.

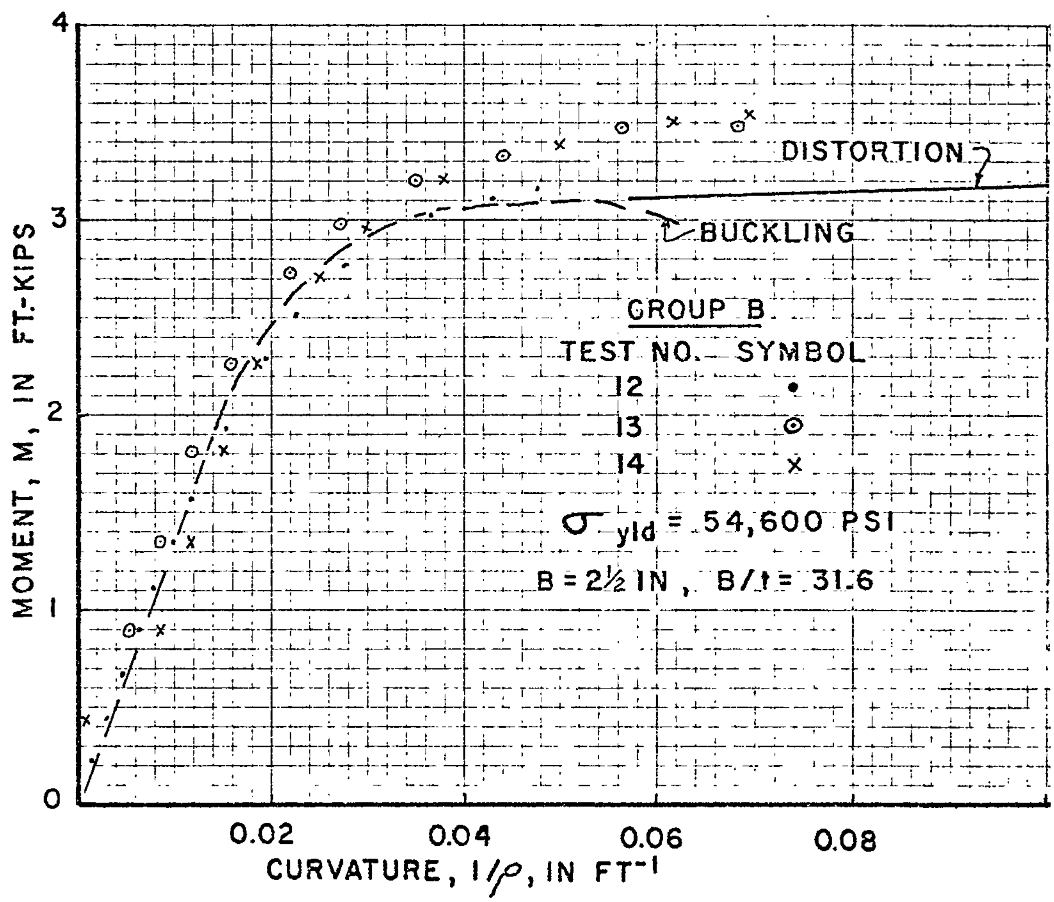

Figure D-2. Moment-Curvature Plots for Specimen Group B.

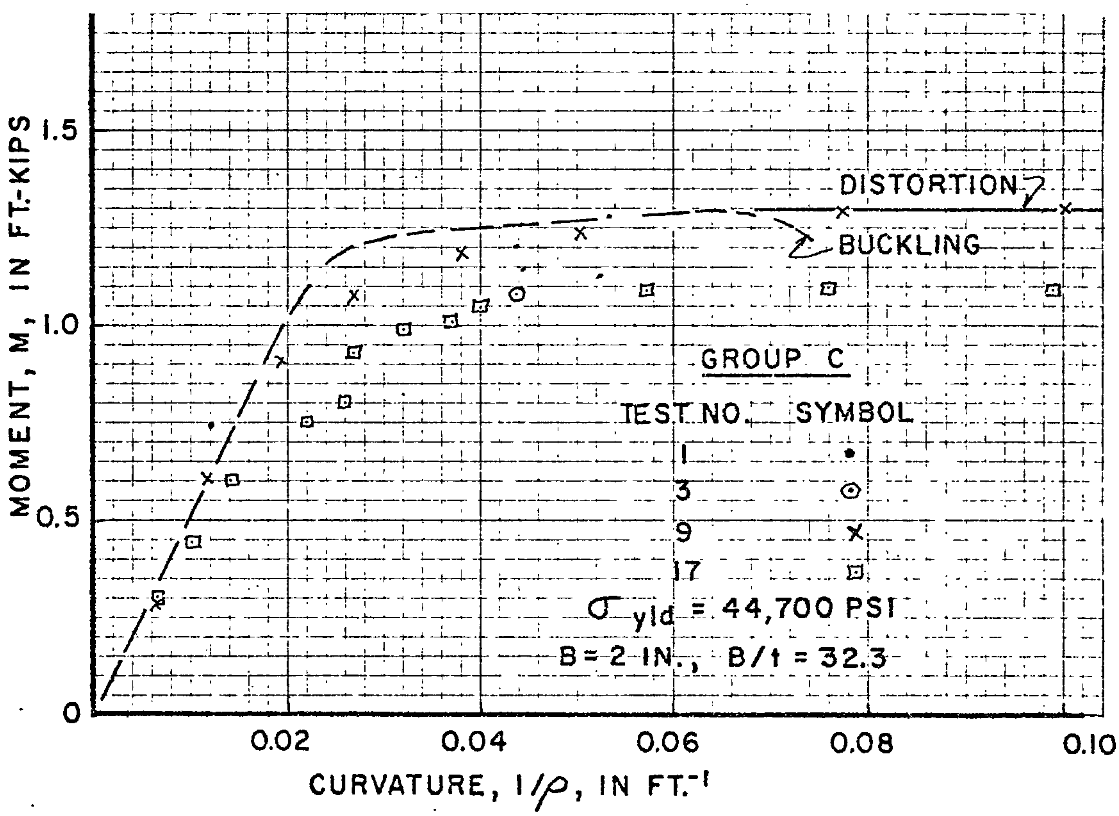

Figure D-3. Moment-Curvature Plots for Specimen Group C.

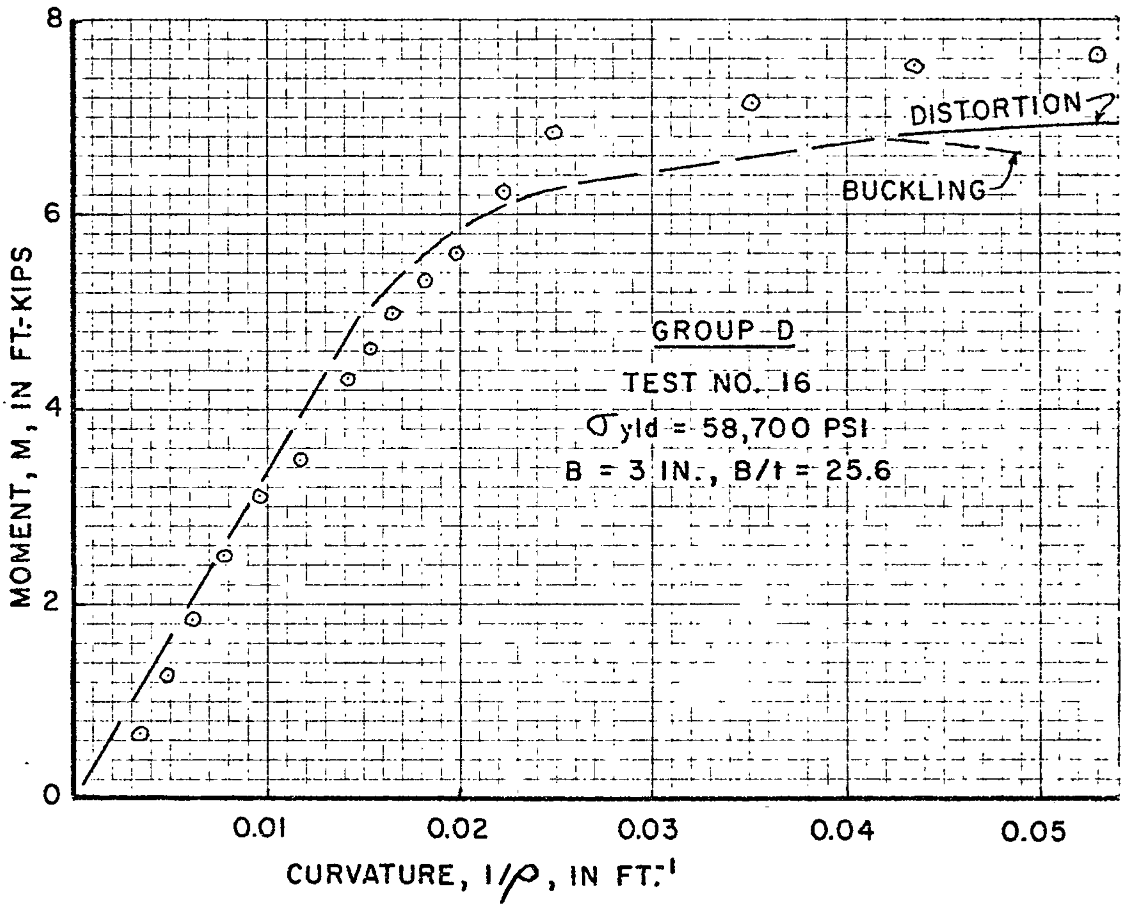

Figure D-4. Moment-Curvature Plots for Specimen Group D.

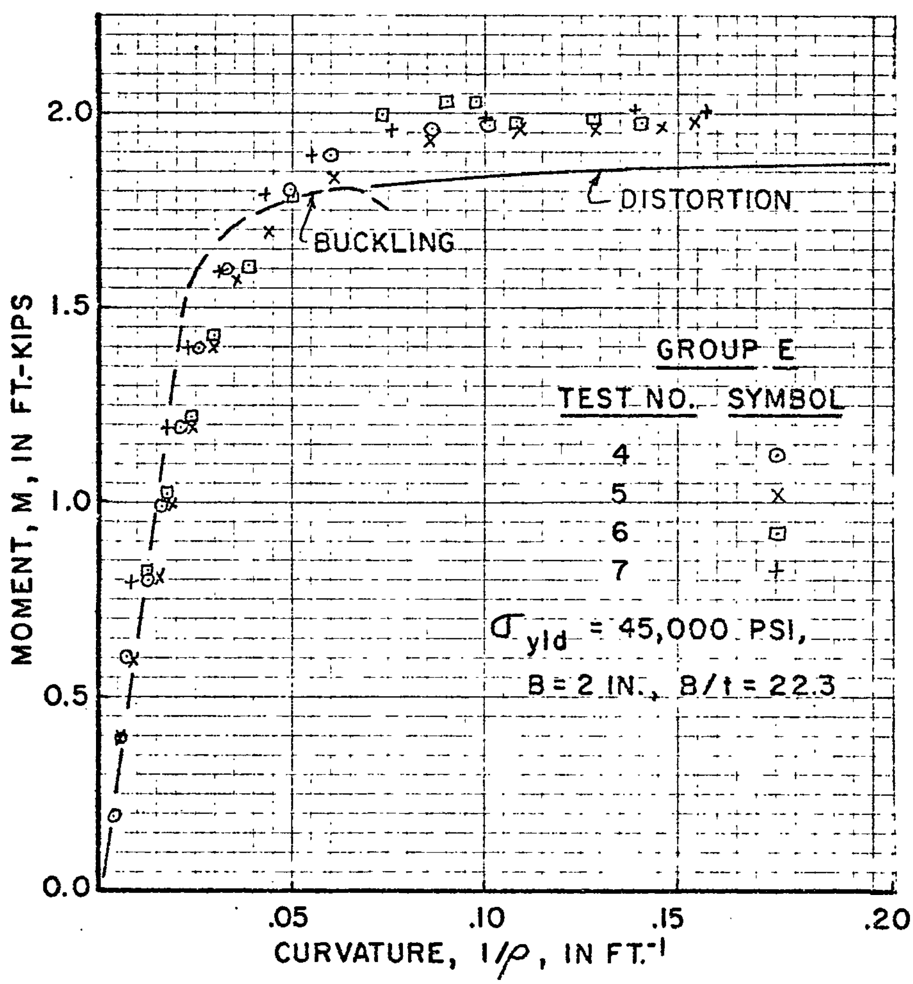

Figure D-5. Moment-Curvature Plots for Specimen Group E.

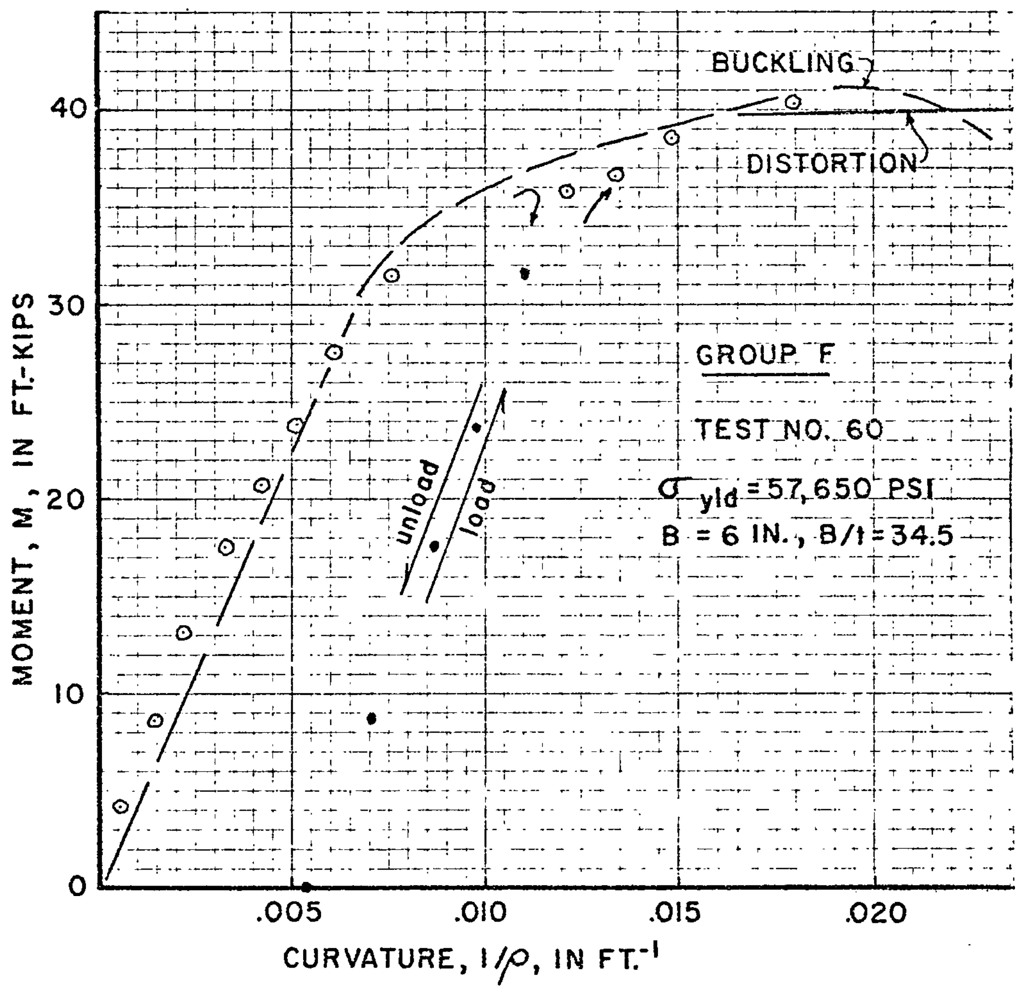

Figure D-6. Moment-Curvature Plots for Specimen Group F.

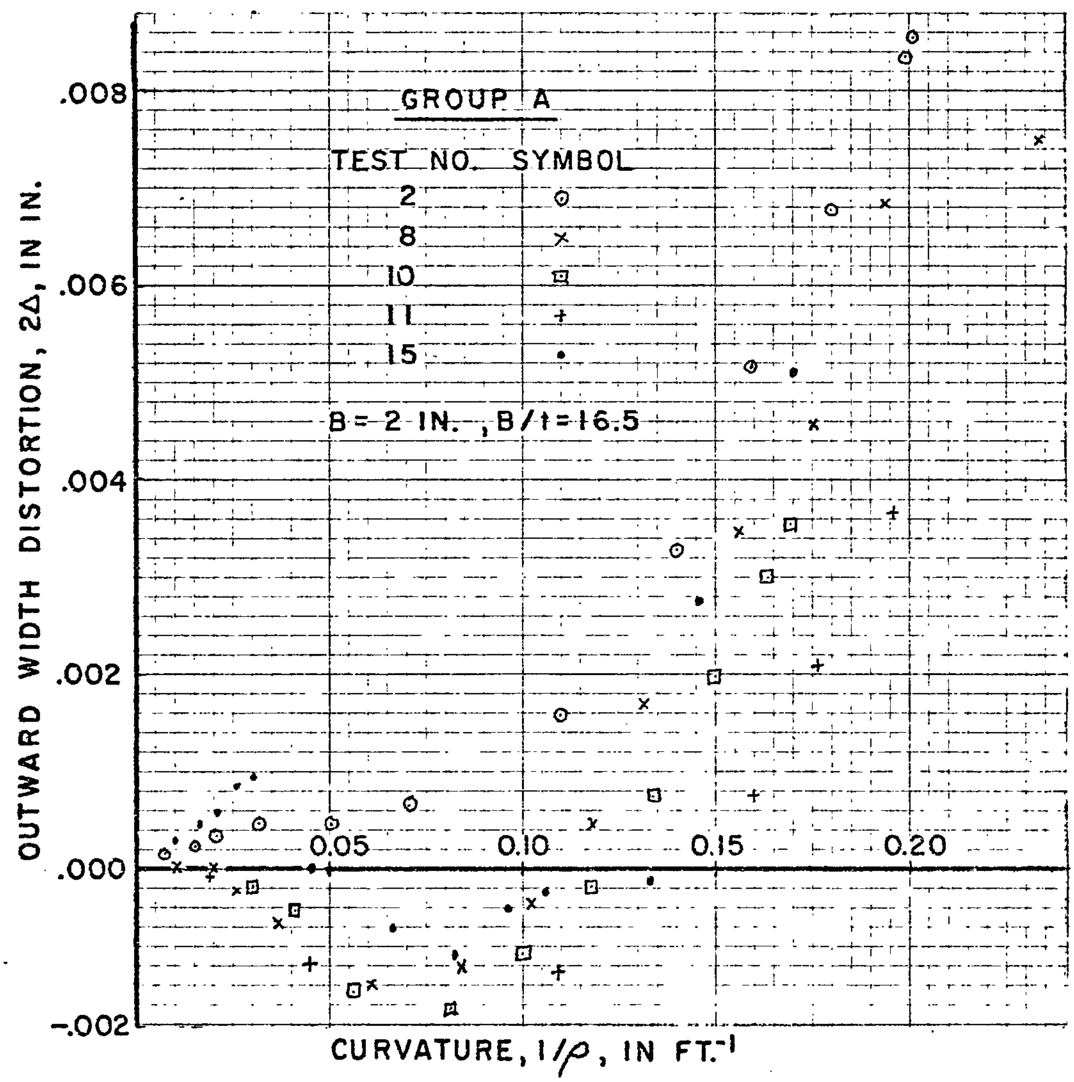

Figure D-7. Distortion-Curvature Plots for Specimen Group A.

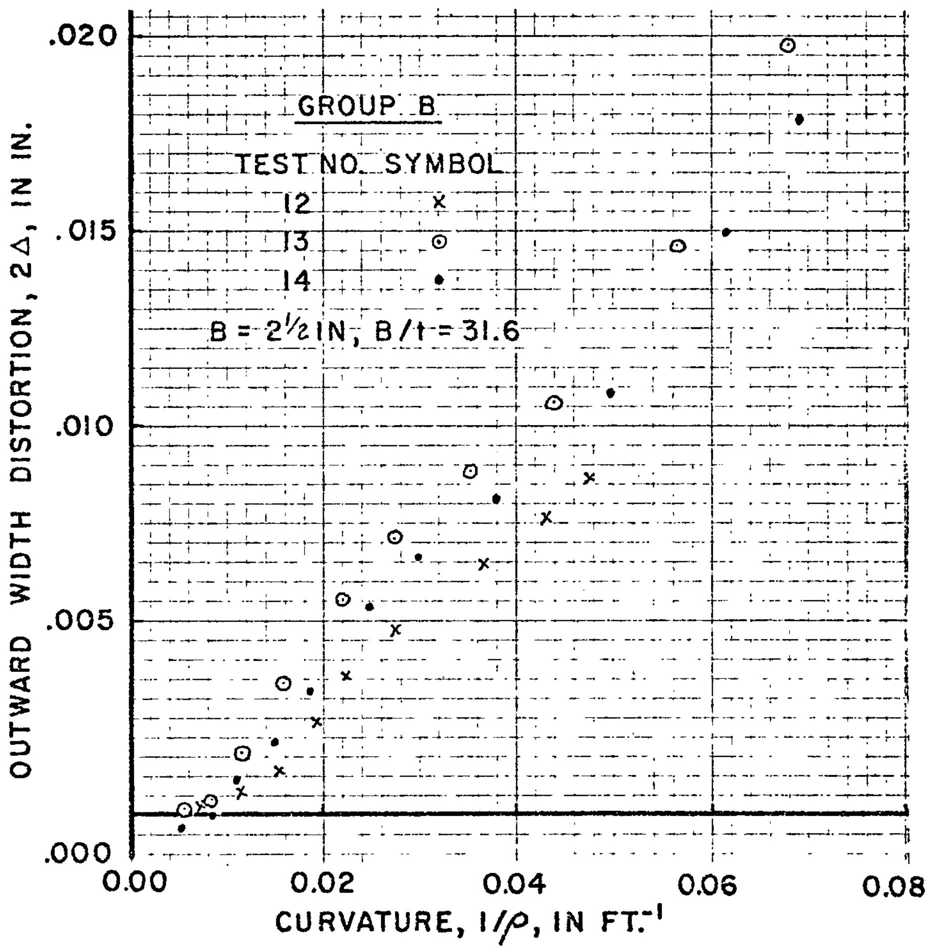

Figure D-8. Distortion-Curvature Plots for Specimen Group B.

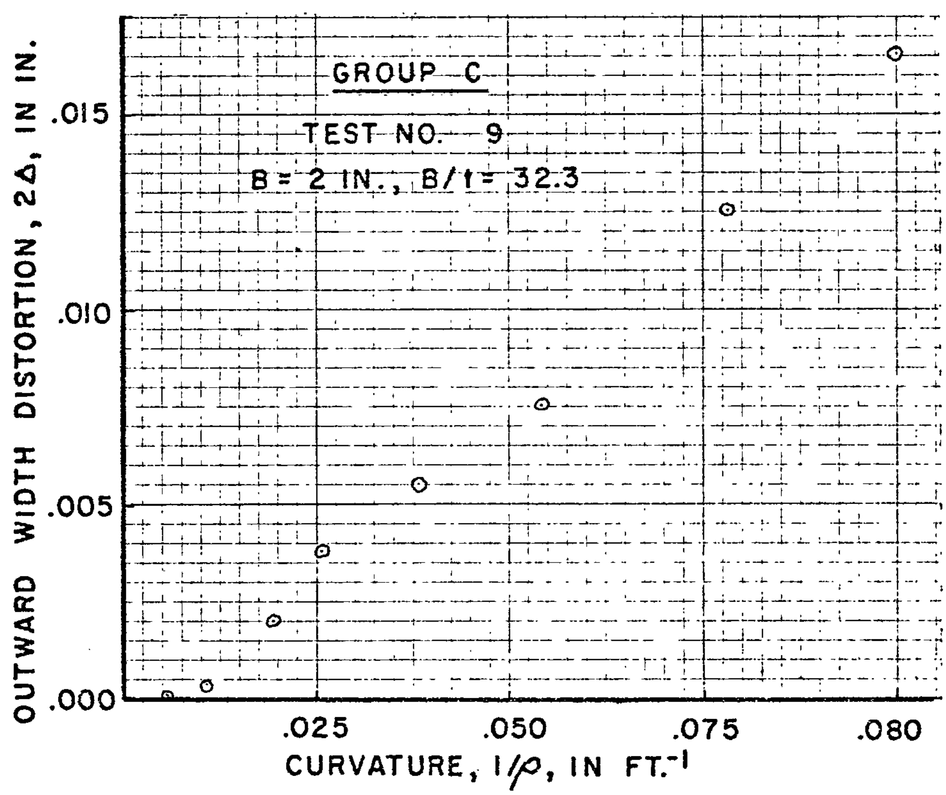

Figure D-9. Distortion-Curvature Plots for Specimen Group C.

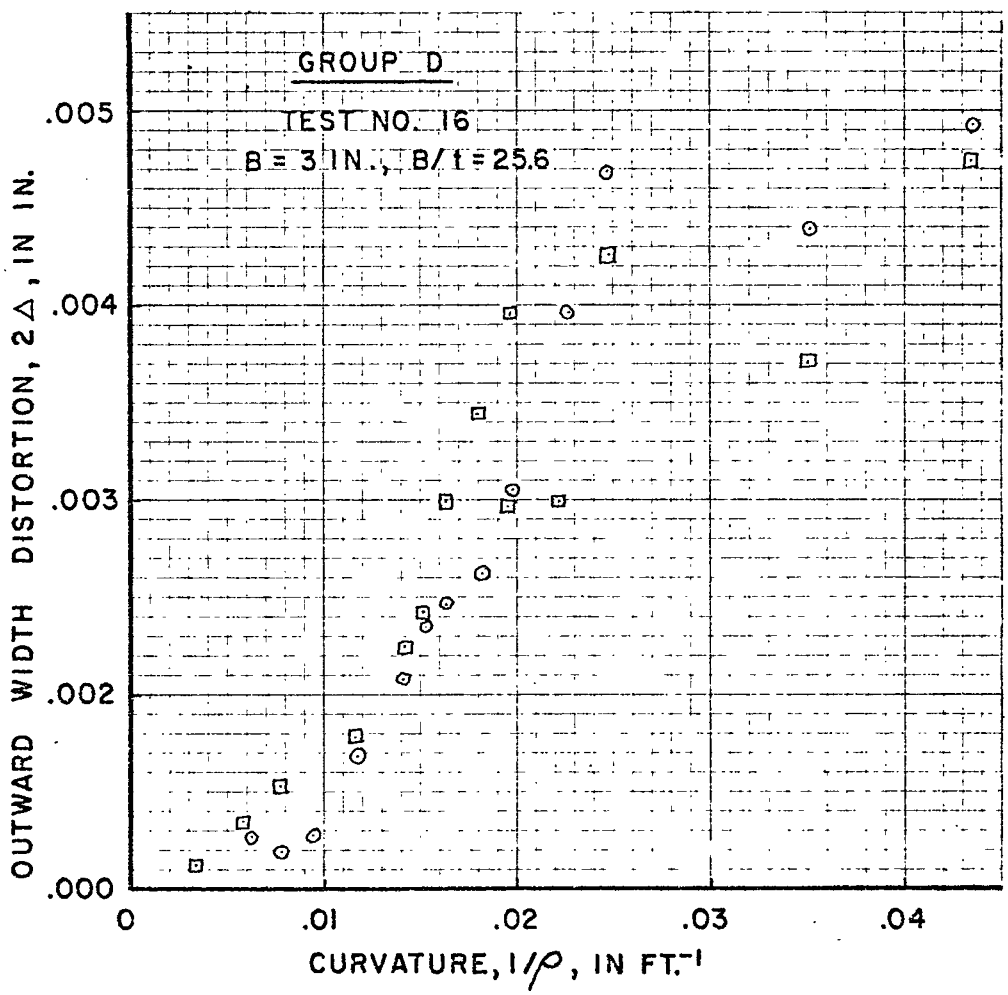

Figure D-10. Distortion-Curvature Plots for Specimen Group D.

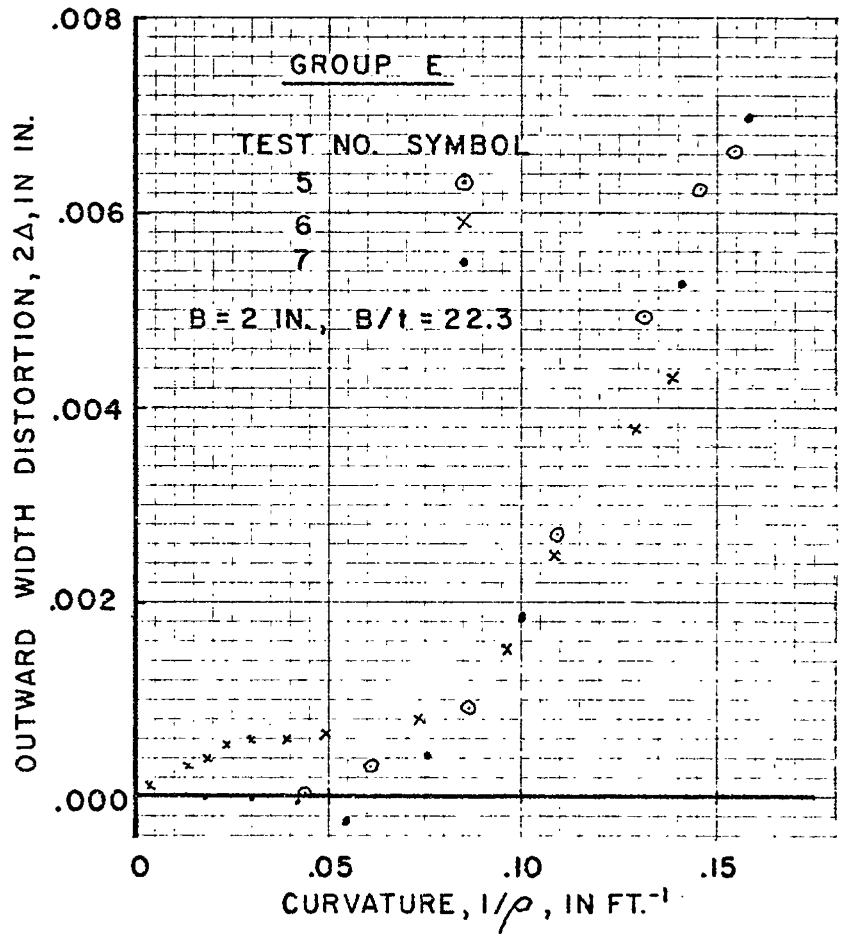

Figure D-11. Distortion-Curvature Plots for Specimen Group E.